Identification of nonlinear modes using phase-locked-loop experimental continuation and normal form

V. Denis *[1], M. Jossic[2], C. Giraud-Audine[3], B. Chomette[2], A. Renault[1] and O. Thomas[1]

[1]Arts et Métiers Paristech, LSIS, UMR CNRS 7296, 8 bd. Louis XIV, 59046 Lille, France
[2]Sorbonne Universités, UPMC Univ Paris 06, UMR CNRS 7190, Institut Jean le Rond d'Alembert, 4 pl. Jussieu, 75252 Paris, France
[3]Arts et Métiers Paristech, L2EP, 8 bd. Louis XIV, 59046 Lille, France

19 janvier 2018

Keywords— distributed nonlinearity, backbone curve, nonlinear mode, nonlinear system identification, phase-locked loop

Abstract

In this article, we address the model identification of nonlinear vibratory systems, with a specific focus on systems modeled with distributed nonlinearities, such as geometrically nonlinear mechanical structures. The proposed strategy theoretically relies on the concept of nonlinear modes of the underlying conservative unforced system and the use of normal forms. Within this framework, it is shown that without internal resonance, a valid reduced order model for a nonlinear mode is a single Duffing oscillator. We then propose an efficient experimental strategy to measure the backbone curve of a particular nonlinear mode and we use it to identify the free parameters of the reduced order model. The experimental part relies on a Phase-Locked Loop (PLL) and enables a robust and automatic measurement of backbone curves as well as forced responses. It is theoretically and experimentally shown that the PLL is able to stabilize the unstable part of Duffing-like frequency responses, thus enabling its robust experimental measurement. Finally, the whole procedure is tested on three experimental systems: a circular plate, a chinese gong and a piezoelectric cantilever beam. It enable to validate the procedure by comparison to available theoretical models as well as to other experimental identification methods.

1 Introduction

The model identification of dynamical systems is an important area of today's research. Basically, it consists in performing dedicated experiments in order to estimate the values of a given set of parameters of an assumed model for the system. In doing so, several goals can be pursued. It may be a simple model validation: one compare the experimentally estimated values of the parameters to the theoretical ones to quantify its closeness to reality. One can also be interested in a model updating: a given set of parameters are left free in the model and their values are estimated with dedicated experiments. For linear systems, modal models are often selected and a large variety of mature and robust parameter identification techniques/algorithms is available [1]. Most of them are implemented in commercial experimental modal analysis software packages. On the contrary, if the system's behaviour involves nonlinearities, the area of system's identification, though extensively addressed in the past twenty years, is still open and no systematic procedure exists. The interested reader is referred to the following review works [2, 3, 4].

The presence of nonlinearities in a given system can dramatically change its behaviour. Among others, the system's free oscillations frequencies, as well as the resonance frequencies, depend on the amplitude. Moreover, some energy exchanges between modes or between distant frequency bands can be observed, leading to harmonic distortion, internal resonances, quasi-periodic oscillations or chaotic oscillations [5]. The physical sources of nonlinearities are numerous, and lead in each case to specific dynamical phenomena. They can be classified

*vivien.denis@ensam.eu

into four families: material nonlinearities (elastoplastic material, nonlinear elastic material...), geometrical nonlinearities (large amplitude oscillations), contact nonlinearities (dry friction, shocks...) and interaction nonlinearities (fluid-structure, electrostatic transduction in micro/nano systems). Until now, the efforts on nonlinear systems identifications have been mainly targeted to localized nonlinearities (almost all the 230 references of the 2016 review [2] are related to localized nonlinearities). By localized, we denote nonlinearities that involve a very small subset of the model's degrees of freedom, the others being linear. Some examples are contact nonlinearities or nonlinearities localized in connection components between subparts of the system.

In the present article, we specifically address the experimental identification of models involving distributed nonlinearities, even if it can be equally applied to models with localized nonlinearities. We target in particular the identification of geometrically nonlinear slender structures, such as beams, plates and shells, with possible interaction nonlinearities such as electrostatic or piezoelectric transductions. Geometrical nonlinearities involve all the model's degrees of freedom (see e.g. [6]), as well as electrostatic transduction, intrinsically nonlinear (see e.g. [7]) and piezoelectric transduction, materially nonlinear for large electric fields [8]. Because of this distributed nature of the nonlinearities, it is impossible to experimentally identify a nonlinear law involving the (numerous) physical degrees of freedom (like a nonlinear stiffness), as often done for localized nonlinearities [2]. Consequently, the method proposed in this article systematically relies on an accurate reduced order model based on the concept of nonlinear modes and normal forms. As introduced for nonlinear structural systems in [9, 10, 11], the normal form theory enables to reduce the dynamics of a nonlinear second order dynamical system to an invariant set of oscillators, each one being associated to a so-called nonlinear mode. If no internal resonance occurs, the system's dynamics in free undamped oscillations can be reduced to a single nonlinear mode, and consequently to a single nonlinear oscillator. Its main characteristics is its hardening / softening behaviour, well defined by its backbone curve, showing the free oscillations frequency as a function of the motion's amplitude. For slender structures such as beams, plates and shells subjected to geometrical nonlinearities, the hardening / softening behaviour of a particular nonlinear mode depends, among other sources, on the curvature (flat structures like beams and plates have always hardening nonlinear modes whereas shells show softening behaviours [12, 13, 14]), on possible prestresses [15] or on electrostatic or piezoelectric interactions [16, 17].

In this article, we propose an efficient strategy to experimentally estimate the backbone curve of a particular nonlinear mode and we use it to identify a reduced order model of the considered nonlinear mode. The experimental identification part relies on a recent measurement technique based on a Phase-Locked Loop (PLL) [18, 19]. The whole procedure is tested on three experimental systems. The first one is a free edge circular plate, already used in [20]. The backbone curves of an axisymmetric mode and two asymmetric companion modes are identified. Then, the estimated parameters are compared to an analytical theoretical model, showing the efficiency of the method, even when 1:1 internal resonance are present. Then, two hardening nonlinear modes of a chinese gong are measured. For those two structures, tested with free edge boundary conditions, the nonlinearities are mainly geometrical. On the contrary, the third tested structure is a piezoelectric cantilever beam, for which the first mode is tested in several electrical conditions. In this latter case, the nonlinearities come from several sources: geometrical, non perfect boundary conditions and piezoelectric material nonlinearities.

2 Nonlinear mode identification

2.1 Nonlinear mode background

2.1.1 First order reduced model

We consider the following N-dimensional model of a nonlinear system, valid for a N degrees of freedom discrete mechanical system or a continuous one, discretized on a N dimensional basis (after a finite element discretization for instance [6, 21]):

$$\boldsymbol{M}\ddot{\boldsymbol{x}} + \boldsymbol{C}\dot{\boldsymbol{x}} + \boldsymbol{K}\boldsymbol{x} + \boldsymbol{f}_{\mathrm{nl}}(\boldsymbol{x}) = \boldsymbol{g}, \tag{1}$$

where $N \in \mathbb{N}$, $\boldsymbol{x}(t)$ is the N dimensional displacement vector, a function of time t, $\boldsymbol{M}$, $\boldsymbol{C}$ and $\boldsymbol{K}$ are the $N \times N$ dimensional mass, damping and stiffness matrices, $\boldsymbol{f}_{\mathrm{nl}}(\boldsymbol{x})$ is the nonlinear part of the internal force vector, $\boldsymbol{g}(t)$ is the external force vector and $\dot{\bullet} = \mathrm{d}\bullet/\mathrm{d}t$. Note that for a sake of simplicity, a linear viscous damping model has been used. We also restrict our attention to geometrically nonlinear structures, for which $\boldsymbol{f}_{\mathrm{nl}}(\boldsymbol{x})$ is a quadratic and cubic polynomial function of $\boldsymbol{x}$ [22, 21, 23].

We first consider a family of $K < N$ linear modes $(\omega_k, \boldsymbol{\Phi}_k)$, $k = 1, \dots K$, solutions of:

$$(\boldsymbol{K} - \omega_k^2 \boldsymbol{M})\boldsymbol{\Phi}_k = \boldsymbol{0}, \tag{2}$$

obtained by considering the eigensolutions of the undamped, free and linearized Eq. (1). Then, we expand the solution $\boldsymbol{x}(t)$ on this basis, i.e. we seek a solution for $\boldsymbol{x}(t)$ of the form:

$$\boldsymbol{x}(t) = \sum_{k=1}^{K} \boldsymbol{\Phi}_k q_k(t). \tag{3}$$

Using the orthogonality properties of the modes, one can show that the modal coordinates $q_k(t)$ verify for all $k = 1, \dots K$:

$$\ddot{q}_k + 2\xi_k \omega_k \dot{q}_k + \omega_k^2 q_k + \sum_{i,j=1}^{K} \beta_{ij}^k q_i q_j + \sum_{i,j,l=1}^{K} \gamma_{ijl}^k q_i q_j q_l = Q_k, \tag{4}$$

with $Q_k = \boldsymbol{\Phi}_k^{\mathrm{T}} \boldsymbol{g} / \boldsymbol{\Phi}_k^{\mathrm{T}} \boldsymbol{M} \boldsymbol{\Phi}_k$ and where the modal damping has been assumed uncoupled (an assumption valid for small damping, even with non proportional $\boldsymbol{C}$ matrix [24]). The values of the nonlinear coefficients β_{ij}^k and γ_{ijl}^k can be computed in practice by several methods (see e.g., among others [25, 23]). The same set of equations is obtained after modal expansions of analytical models of beams, plates and shells [5, 26, 13, 27].

To this end, the model size has been reduced from N to K (with, hopefully, $K \ll N$). However, in practice, the choice of the linear mode basis (the K retained linear modes) is not an easy task and a further reduction of the model size can be done with the help of the nonlinear mode framework. In the same way than for defining the linear modes (Eq. (2)), we consider the underlying conservative model (4) in free vibrations ($\xi_k = Q_k = 0$ $\forall k$). Using normal forms, as introduced in [9, 10, 28], it is possible to simplify model (4) by introducing the following nonlinear change of coordinates, for all $k = 1, \dots K$:

$$q_k = u_k + \mathcal{P}_k^{(2)}(u_i, \dot{u}_i) + \mathcal{P}_k^{(3)}(u_i, \dot{u}_i), \tag{5}$$

where $\mathcal{P}_k^{(p)}(u_i, \dot{u}_i)$, $i = 1, \dots K$, is a polynomial function of $(u_i, \dot{u}_i)$ containing monomial terms of order p only (For instance, for $p = 2$ and $K = 2$, the monoms of $\mathcal{P}_k^{(2)}$ are u_1^2, $u_1 u_2$, u_2^2, $\dot{u}_1^2$, $\dot{u}_1 \dot{u}_2$, $\dot{u}_2^2$ [10]). By substituting q_k for u_k in Eq. (4) using Eq. (5), it is possible to choose the coefficients of the monomials of $\mathcal{P}_k^{(p)}(u_i, \dot{u}_i)$ in order to cancel most of the nonlinear terms in (4). More precisely, all the non resonant nonlinear terms can be cancelled. Nonlinear monomials are often resonant because of the occurrence of internal resonances. Some others are naturally resonant (it is the case for some cubic ones), i.e. without the occurrence of a particular internal resonance (see [5, 10] for details about internal resonances and resonant terms). If we assume here that there are no internal resonances, the initial dynamical system (4) is replaced by the following one, for all $k = 1, \dots K$:

$$\ddot{u}_k + \omega_k^2 u_k + \mathcal{Q}_k^{(3)}(u_i, \dot{u}_i) = 0, \tag{6}$$

in which $\mathcal{Q}_k^{(3)}(u_i, \dot{u}_i)$, $i = 1, \dots K$ denotes a polynomial function of $(u_i, \dot{u}_i)$ of order 3 only. All coefficients of the monomials of $\mathcal{P}_k^{(p)}$ and $\mathcal{Q}_k^{(3)}$ are formally known as functions of the coefficients β_{ij}^k and γ_{ijl}^k of the initial dynamical system (4) [10].

This new dynamical system (6) is called the normal form of the initial one (4) and has two interesting properties. First, it involves much less nonlinear monomials. In particular, all quadratic terms have been cancelled, since they are all non-resonant, and it remains only cubic terms. Second, the only remaining (cubic) nonlinear terms are such that they don't break the invariance of the oscillators of the normal form (6). It means that if a particular motion is initiated on a particular normal oscillator only, no energy is given to the others such that the motion remains on this oscillator only. Mathematically, if the motion is initiated on the i-th. normal coordinate, at $t = 0$ $u_i \neq 0, \dot{u}_i \neq 0$ and for all the others the initial conditions are zero: $u_j = 0, \dot{u}_j = 0$, $\forall j \neq i$, then this latter property remains for all $t > 0$. In the K-dimensional phase space, the trajectory of the solution $q_k(t)$ $\forall k$ remains on a curved manifold (called the i-th invariant manifold), which is tangent to the i-th linear eigen-plane around the equilibrium point $q_k = 0$ $\forall k$. These properties lead to the concept of a nonlinear normal mode (NNM), here defined as an invariant manifold of the phase space, for which the above normal form theory enables to directly compute the oscillations by using (6). Moreover, the geometry of the curved manifold is defined by the nonlinear change of variables (5).

If a nonlinear modal motion on the i-th NNM is considered, $u_j = 0, \dot{u}_j = 0$, $\forall j \neq i$ and the normal dynamics (6) reduces to [10]:

$$\ddot{u}_i + \omega_i^2 u_i + \Gamma_1 u_i^3 + \Gamma_2 u_i \dot{u}_i^2 = 0, \tag{7}$$

where Γ_1 and Γ_2 are the coefficients of the third order polynomial $\mathcal{Q}_i^{(3)}(u_i, \dot{u}_i)$, functions of the β_{ij}^k and γ_{ijl}^k [10]. In addition to the classical "Duffing" cubic nonlinear term $\Gamma_1 u_i^3$, the normal form adds another cubic term $\Gamma_2 u_i \dot{u}_i^2$. This equation is exact up to the order 3 in $(u_i, \dot{u}_i)$, since Eqs. (5) and (6) are obtained after truncated asymptotic expansions. It defines the nonlinear free oscillations on the i-th. NNM and in particular the dependence of the free oscillation frequency $\omega_{\rm nl}$ as a function of the amplitude (energy) of the motion, often referred as the backbone curve [5] or the frequency - energy plot [29]. A first order perturbative solution of (7) leads to:

$$u_i(t) = \epsilon a_1 \cos(\omega_{\rm nl} t + \varphi), \tag{8}$$

with [10]

$$\omega_{\rm nl} = \omega_i \left(1 + T\epsilon^2 a_1^2\right) \quad \text{and} \quad T = \frac{3\Gamma_1 + \Gamma_2 \omega_i^2}{8\omega_i^2}, \tag{9}$$

where $\epsilon \ll 1$ is a bookkeeping symbol to remind that the amplitude ϵa_1 of the motion needs to be small for the above expressions to be valid. The so-called backbone curve is obtained by plotting $\omega_{\rm nl}$ as a function of ϵa_1.

To observe this particular "one NNM" motion in the physical space, one can introduce $u_i(t)$ defined by Eq. (8) into the nonlinear change of variables (5), to obtain:

$$q_i(t) = u_i(t) + o(\epsilon^2), \quad q_j(t) = o(\epsilon^2), \quad \forall j \neq i, \tag{10}$$

so that, back to Eq. (3), one shows that:

$$\boldsymbol{x}(t) = \boldsymbol{\Phi}_i u_i(t) + \boldsymbol{o}(\epsilon^2) \simeq \boldsymbol{\Phi}_i \epsilon a_1 \cos(\omega_{\rm nl} t + \varphi). \tag{11}$$

The above equation (11) shows that at first order, i.e. for small oscillations amplitude, the only nonlinear effect is the free oscillation frequency dependence upon the motion amplitude. Conversely, the motion onto one NNM is synchronous and has the shape of the i-th mode shape. As shown in a series of article [10, 30, 11, 14], the present normal form approach is very efficient to predict the right hardening / softening trend of a particular NNM, defined by coefficient T of Eq. (9), since coefficients Γ_1 and Γ_2 are functions of all the β_{ij}^k and γ_{ijl}^k and thus embed the non resonant effect of all the K linear modes of Eq. (4).

When forced oscillations are considered, the normal form (8) can still be considered (and valid at first order [31]), by adding damping and forcing terms of the initial dynamical system (4):

$$\ddot{u}_i + 2\xi_i \omega_i \dot{u}_i + \omega_i^2 u_i + \Gamma_1 u_i^3 + \Gamma_2 u_i \dot{u}_i^2 = Q_i. \tag{12}$$

The above equation thus enables to predict the forced resonant oscillations of the system in the frequency vicinity of the i-th. NNM.

2.1.2 Higher order effects

To consider higher order effects, that emerge for higher motion amplitude, we correct the result of Eq. (8) by adding more harmonics. Since the nonlinearity in Eq. (7) is odd, the constant and second harmonics have a zero amplitude, so that a higher order perturbative development gives:

$$u_i(t) = \epsilon a_1 \cos\phi + \epsilon^3 a_3 \cos 3\phi, \tag{13}$$

with $\phi = \omega_{\rm nl} t + \varphi$. Following the same approach, Eq. (11) is replaced by:

$$\boldsymbol{x}(t) = \epsilon^2 \sum_{k=1}^{K} \boldsymbol{\Phi}_k b_{k0} + \epsilon \cos\phi \left[\boldsymbol{\Phi}_i b_{i1} + \epsilon^2 \sum_{\substack{k=1 \\ i \neq k}}^{K} b_{k1} \boldsymbol{\Phi}_k \right] + \epsilon^2 \cos 2\phi \sum_{k=1}^{K} \boldsymbol{\Phi}_k b_{k2} + \epsilon^3 \cos 3\phi \sum_{k=1}^{K} \boldsymbol{\Phi}_k b_{k3} + \boldsymbol{o}(\epsilon^4). \tag{14}$$

where the b_{kh}, $k = 1 \ldots K$ and $h = 1, 2, 3$ depend on a_1, a_3 and the change of variables (5). One can observe two effects of the higher order nonlinearities. Firstly, they bring supplementary harmonics in the signal. The continuous (H0) and second (H2) harmonics are the direct consequence of the polynomial $\mathcal{P}_k^{(2)}$ in the change of variables (5). The third (H3) harmonics is the conjoint consequence of the polynomial $\mathcal{P}_k^{(3)}$ and the third harmonics in the normal coordinate u_i (Eq. (13)), the latter created by the nonlinear normal dynamics (terms u_i^3 and $u_i \dot{u}_i^2$ in Eq. (7)). Secondly, the deformed shape of $\boldsymbol{x}(t)$ depends on the motion amplitude and on time (the motion is no more synchronous since it depends on the contribution of all the deformed shapes $\boldsymbol{\Phi}_k$ in a time-dependent manner). Indeed, even if the dynamical deformed shape of the NNM is mainly governed by $\boldsymbol{\Phi}_i$, oscillating at H1 at order ϵ, it is corrected by second order terms in ϵ^2, ϵ^3, proportional to the other mode shapes $\boldsymbol{\Phi}_k$, $k \neq i$. However, those two nonlinear manifestations are of the second order with respect to the free oscillation frequencies and are for this reason neglected in the following.

2.1.3 Comparison with other theories

The normal form approach introduced in the previous section leads to naturally define a NNM as an invariant solution of the underlying unforced conservative system (Eq. (1) with $\boldsymbol{C} = \boldsymbol{0}$ and $\boldsymbol{g} = \boldsymbol{0}$). Since the obtained solution moves on an invariant manifold of the phase space, the present approach is equivalent to the one introduced by Shaw and Pierre, who defined a NNM as an invariant manifold of the phase space [32, 33]. Equivalently, other authors ([29] and reference therein) extended the initial definition of Rosenberg [34] and defined a NNM as a periodic solution of the conservative system in free oscillations. Since a periodic orbit is by nature invariant, this second definition implies the first one. Conversely, theorems due to Lyapunov [35, pp. 361, 386] and Kelley [36] show that any smooth nonlinear N degrees of freedom 2nd. order conservative dynamical system presents N families of periodic orbits around any stable equilibrium point, which coincide with the invariant manifolds. All those definitions of a NNM are thus equivalent and all address the same concept. On the contrary, the extension of the nonlinear mode concept to damped systems is still under extensive research (see e.g. [28, 37]).

2.2 Nonlinear mode identification

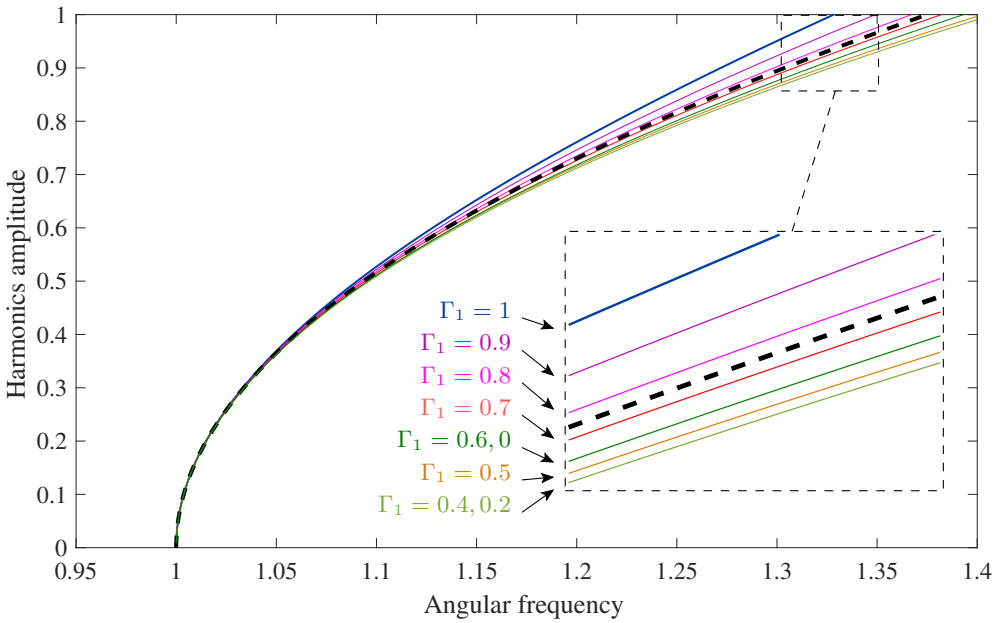

Figure 1 – Backbone curves: amplitude of the first harmonic (corresponding at first order to ϵa_1) of the response as a function of the oscillation frequency $\omega_{\text{nl}}/\omega_i$ of oscillator (7) solved with ANM/HBM. Nine values of (Γ_1, Γ_2) are considered as specified on the figure: $\Gamma_1 \in \{1, 0.9, 0.8, 0.7, 0.6, 0.5, 0.4, 0.2, 0\}$ and $\Gamma_2 \in \{0, 0.3, 0.6, 0.9, 1.2, 1.5, 1.8, 2.4, 3\}$, respecting $\Gamma_0 = \Gamma_1 + \Gamma_2\omega_i^2/3 = 1$. The solution at first order for $\Gamma_0 = 1$ is also plotted (dashed black).

A first and basic idea to identify the model would be to experimentally estimate all the $\beta_{ij}^k, \Gamma_{ijl}^k$ coefficients of the modal model (4). Considering the huge amount of coefficients (for a $N = 10$ degrees of freedom model, the model involves $N^3 = 10^3$ β_{ij}^k and $N^4 = 10^4$ Γ_{ijl}^k coefficients.), this is an impossible task in practice. In contrast, the idea proposed in this article is to use the power of the normal form approach.

Using normal forms to exhibit a reduced order model that is then identified using experiments has been considered in the past in the case of internal resonances in plates and shells [20, 38, 39]. Here, we restrict ourselves on only one NNM, characterized at first order by the normal form written in Eq. (7). We then propose here to characterize and identify this NNM by experimentally identifying the values of the parameters of Eq. (7), namely the linear oscillation frequency (or eigenfrequency) ω_i and the nonlinear coefficients Γ_1, Γ_2. In practice, we propose to identify the NNM model by measuring the backbone curve.

At first order, the backbone curve is equivalent to a parabola in the plane $(\omega_{\text{nl}}, \epsilon a_1)$, of equation (9), whose curvature is given by T which depends on the two nonlinear coefficients Γ_1 and Γ_2. Consequently, an infinite number of values of (Γ_1, Γ_2) leads to the same value of T and thus, at first order, to the same backbone curve. Fig. 1 shows several backbone curves for 9 values of (Γ_1, Γ_2) leading to the same value of T and numerically

computed with the software Manlab with the Harmonic Balance Method and the asymptotic numerical method (HBM/ANM). It enables the numerical continuation of periodic solutions ([40]). The simulations of Fig. 1 can be considered as a reference since 12 harmonics have been used. They show that under a reasonably high amplitude range ($a < 0.5$), all the curves are merged with a single parabola, so that they are all equivalent to the solution of a classical Duffing oscillator:

$$\ddot{u}_i + \omega_i^2 u_i + \Gamma_0 u_i^3 = 0, \tag{15}$$

with

$$\Gamma_0 = \frac{8\omega_i^2 T}{3} = \Gamma_1 + \frac{\Gamma_2 \omega_i^2}{3}. \tag{16}$$

Since we are interested in a first order identification of a NNM, we propose here to simply characterize a NNM by the Duffing oscillator of Eq. (15), which is able to efficiently capture the first order behaviour of the NNM. We then identify Γ_0 (which embeds the effect of Γ_1 and Γ_2) by fitting a parabola on the experimental backbone curve.

Figure 1 also shows that the differentiated effect of Γ_1 and Γ_2 appears at higher amplitudes. It would be theoretically possible to fit an order four polynomial on the curves to separately identify Γ_1 and Γ_2. This point is left out of the scope of the present paper.

It is widely known [5] that the incurvation of the backbone curve, the so called hardening / softening behaviour of the considered mode, is associated to the order of nonlinearities: a hardening behaviour comes from cubic nonlinearities while a softening behaviour is due to quadratic nonlinearities. One can remark that Eq. (7) only uses cubic coefficients. It is in fact a consequence of the normal form theory and the cubic coefficients Γ_1 and Γ_2 embed both the quadratic and cubic nonlinearities appearing the equations of motion of the dynamical system [10]. Using this formalism, the type of nonlinearity is still indicated by the incurvation of the backbone through the sign of T or Γ_0. If $\Gamma_0 < 0$ the NNM is softening while it is hardening if $\Gamma_0 > 0$.

2.3 Some particular properties

As seen previously, we propose to identify a nonlinear mode as the Duffing oscillator (15) using its backbone curve, which is its solution in free vibrations. In practice, as seen in the following, some experimental procedure will rely on a forced excitation of the system. This section clarifies the concepts of amplitude resonance, phase resonance and their relations to particular points of the free and forced frequency responses of a Duffing oscillator.

We consider the following forced Duffing oscillator associated to Eq. (12) with $u \equiv u_i$, $\omega_0 \equiv \omega_i$, $\xi \equiv \xi_i$, $Q \equiv Q_i$ and Γ_0 defined by Eq. (16):

$$\ddot{u} + 2\xi\omega_0 \dot{u} + \omega_0^2 u + \Gamma_0 u^3 = Q. \tag{17}$$

To consider universal results, it is worth noting that (17) can be rescaled in amplitude and time by defining:

$$\bar{t} = \omega_0 t, \quad \bar{u} = \frac{\sqrt{\Gamma_0}}{\omega_0} u, \tag{18}$$

to obtain the following equation:

$$\ddot{\bar{u}} + 2\xi\dot{\bar{u}} + \bar{u} + \bar{u}^3 = \bar{Q}, \tag{19}$$

with $\dot{\bar{u}} = \mathrm{d}\bar{u}/\mathrm{d}\bar{t}$. The above equations show that the forced response of any Duffing oscillator qualitatively depends on two parameters only: the damping factor ξ and the forcing $\bar{Q}$. In free oscillations, no free parameters remain after the scaling, so that the free response of any Duffing oscillator can be displayed by a single backbone curve, provided the scaling of Eq. (18) is applied. In the following, we shall equivalently consider Eq. (17) with $\Gamma_0 = 1$ and study its response as a function of frequency $\bar{\Omega} = \Omega/\omega_0$ in the frequency domain.

When measuring the response of Eq. (17) in free or forced vibrations, several particular behaviours can be considered.

2.3.1 Phase resonance

The phase resonance is first considered. It is the particular case for which the excitation term $Q(t)$ in Eq. (17) exactly cancels, for all time t, the damping term $2\xi\omega_0\dot{u}$, so that the oscillator behaves as if it was in undamped free oscillations. For a linear oscillator ($\Gamma_0 = 0$) it is well known [41, 24] that a sine forcing $Q(t) = Q_0 \cos\Omega t$ with $\Omega = \omega_0$ achieves this goal. In this case, the displacement $u(t)$ is in phase quadrature with $Q(t)$ (if $u(t) = u_0\cos(\Omega t + \varphi)$, $\varphi = -\pi/2$). In the nonlinear case, since the solutions of Eq. (17) are periodic but often multiharmonic, it is shown in [42] that the same result is obtained by balancing each harmonic of the damping term by a corresponding harmonic in the forcing. More precisely, we look at the solution of Eq. (17) under a monophase periodic motion, with a phase lag of $\pi/2$ with respect to the periodic forcing:

$$u(t) = \sum_{h=1}^{+\infty} u_h \cos h\Omega t, \quad Q(t) = \sum_{h=1}^{+\infty} Q_h \sin h\Omega t. \tag{20}$$

The time derivatives of $u(t)$ and $u^3(t)$ can be written:

$$\dot{u}(t) = -\sum_{h=1}^{+\infty} h\Omega u_h \sin h\Omega t, \quad \ddot{u}(t) = -\sum_{h=1}^{+\infty} h^2\Omega^2 u_h \cos h\Omega t, \quad u^3(t) = \sum_{h=1}^{+\infty} w_h(u_i) \cos h\Omega t, \tag{21}$$

where $w_h(u_i)$ is the h-th. harmonics of u^3 that depends on u_i, $i \in \mathbb{N}^*$. Introducing the above Fourier series expansions in Eq. (17) and balancing the sine and cosine terms (i.e. applying the harmonic balance method) leads to, for all $h \in \mathbb{N}^*$:

$$\begin{cases} \left(\omega_0^2 - h^2\Omega^2\right) u_h + \Gamma_0 w_h(u_i) = 0, & (22) \\ -2h\xi\omega_0\Omega u_h = Q_h, & (23) \end{cases}$$

equations being equivalent in pairs to:

$$\begin{cases} \ddot{u} + \omega_0^2 u + \Gamma_0 u^3 = 0, & (24) \\ -2\xi\omega_0\dot{u} = Q. & (25) \end{cases}$$

Eq. (24) is exactly the underlying undamped free oscillator, equivalent by definition to the nonlinear mode. Its solution (obtained by solving Eqs. (22)) gives the frequency of oscillations and the amplitude of each harmonics as a function of the first one ($\Omega = \omega_{\mathrm{nl}} = f(u_1)$, $u_h = f(u_1)\ \forall h > 1$), the so-called backbone curve. Then, Eq. (23) gives the value of the forcing harmonics as a function of u_h to exactly balance the damping term $2\xi\omega_0\dot{u}$.

As a conclusion, the above considerations show that it is possible to choose the shape of the forcing signal $Q(t)$ so that it exactly balance the damping term, implying that the oscillations $u(t)$ are those of the underlying undamped and unforced oscillator, equivalent to oscillations on the nonlinear mode. In practice, one has to find the frequency $\Omega = \omega_{\mathrm{nl}}$ and the right amplitude of Q_h for which the phase lag of each harmonics of $Q(t)$ with respect to the corresponding one of $u(t)$ is $\pi/2$.

In practice, however, as shown by Eq. (13), the higher harmonics of $u(t)$ (and thus of $\dot{u}$) are often much smaller than the first one, so that considering the following single sine signal for $Q(t)$:

$$u(t) \simeq u_1 \cos\omega_{\mathrm{nl}} t \quad \Rightarrow \quad Q(t) = -2\xi\omega_0\omega_{\mathrm{nl}} u_1 \sin\omega_{\mathrm{nl}} t, \tag{26}$$

is a practical excellent application of the phase resonance. One has consequently to apply a $\pi/2$ phase lag between the first harmonics of $Q(t)$ and $u(t)$ and plot the oscillations frequency $\Omega = \omega_{\mathrm{nl}}$ as a function of u_1 to obtain the backbone curve of the nonlinear mode.

2.3.2 Frequency response

Fig. 2 shows the frequency response of the Duffing oscillator (17) for $\Gamma_0 = 1$ and $\xi = 0.1$. They are numerically obtained with the harmonic balance method and the Asymptotic Numerical Method (HBM/ANM), implemented in the software package Manlab [40], which enable the continuation of periodic solutions of (17), by computing the Fourier coefficients of $u(t)$:

$$u(t) = u_0 + \sum_{h=1}^{H} \left(u_h^c \cos h\Omega t + u_h^s \sin h\Omega t\right) = u_0 + \sum_{h=1}^{H} u_h \cos(h\Omega t + \varphi_h). \tag{27}$$

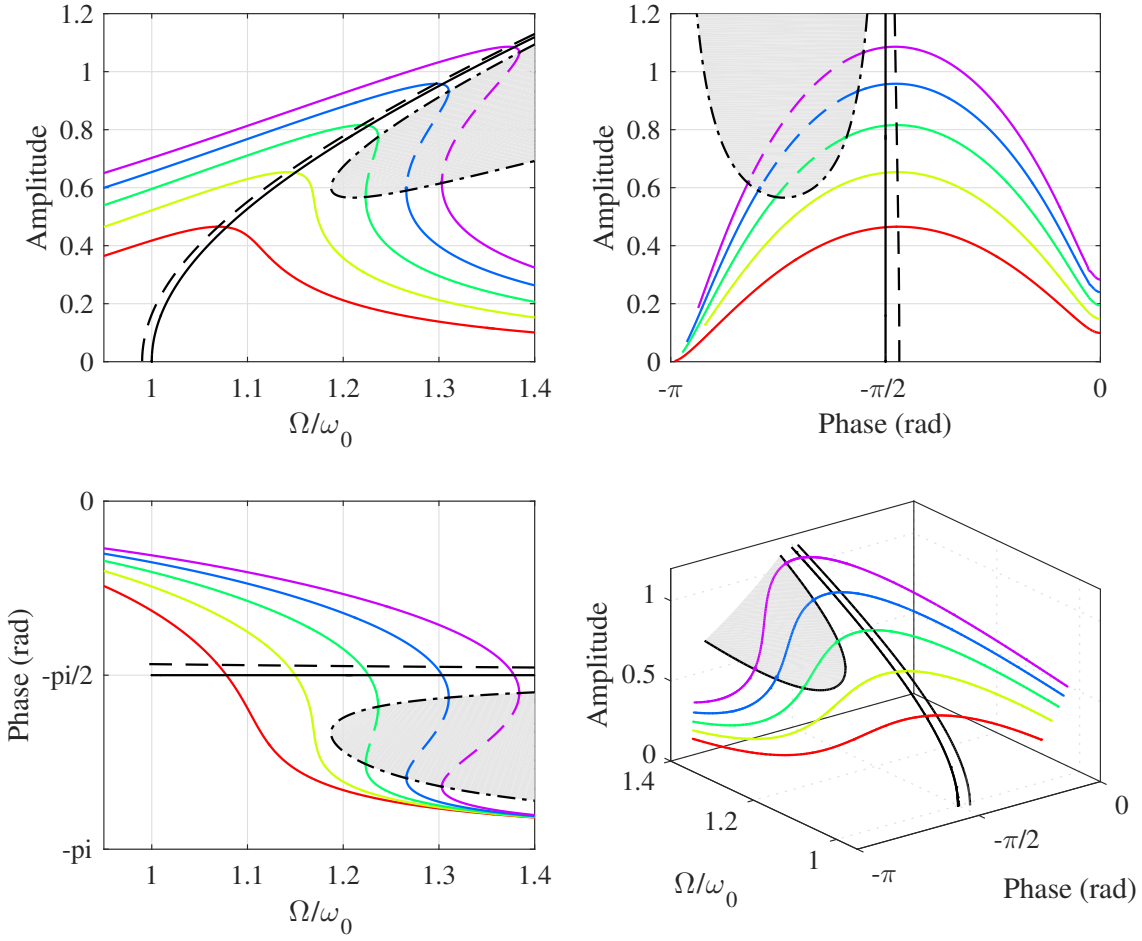

Figure 2 – Frequency responses (thin rainbow lines, F=0.1 0.15 0.2 0.25 0.3), continuation of the amplitude (dashed black line) and phase (solid black line) resonances, and continuation of the fold point (dash-dotted black line) for the system (17).

Since a large number of harmonics H is taken into account, the obtained plots can be considered as reference solutions. Fig. (2) shows the amplitude and phase of the first harmonics ($u_1 = \sqrt{(u_1^c)^2 + (u_1^s)^2}, \varphi_1 = -\operatorname{atan}(u_1^s/u_1^c)$) as a function of Ω/ω_0. A number of remarkable properties of this frequency response can be drawn.

- The forced frequency response curves are the solutions of (17) with $Q(t) = Q_1 \cos \Omega t$. They are shown in colored lines, for different forcing amplitudes Q_1. The dashed part of the curves indicates the unstable region, associated to the multivalued parts of the curves, which leads to the jump phenomenon.
- The backbone curve, equivalent to a phase resonance, is computed by solving Eq. (17) in undamped free oscillations. It is shown in solid black line and is precisely associated to a $\varphi = -\pi/2$ phase lag between $u(t)$ and $Q(t)$.
- The amplitude resonance, which is the locus of the maxima of amplitude of each frequency response, is obtained by numerically following a singular point of the frequency-amplitude function [43, 44]. It is plotted in dashed black line.
- The locus of the saddle-node bifurcation, delimiting the jump-down and the unstable region, is obtained by numerically following a singular point of amplitude-frequency function [43, 44] and is plotted in dash-dotted black.

It is remarkable that for a damped system, the backbone curve – equivalent to a phase resonance and obtained either by locking on the phase resonance or by following the free oscillations – is distinct from the amplitude resonance, obtained by interpolating the maxima of amplitude of the frequency responses. Note that this difference also exists in the case of a linear damped system. This difference is here displayed for moderately damped system (the figure corresponds to $\xi = 0.1$) and should be negligible for lightly damped systems. Often

in the literature, this difference is neglected because analytical solutions obtained by a first order perturbative solution give equal amplitude and phase resonances. One can notice that the backbone curve is located between the amplitude resonance and the upper saddle node bifurcation, close to the right (upper frequencies) of the maxima, and always in the stable region.

Another remarkable result shown on Fig. 2 is that the phase φ_1 is a monotonous decreasing function of the forcing frequency Ω, whereas the amplitude u_1 is multivalued.

2.4 Experimental strategies

Experimentally, the easiest way to obtain an estimation of the backbone curve is to measure several frequency responses for different vibration amplitudes and to seek the amplitude resonance as the locus of the maxima of the responses. The frequency response around resonance for a given amplitude is obtained by exciting at a given frequency, waiting for the steady state regime, recording the amplitude of motion, increasing or decreasing the frequency by a small step, and repeating until the forced response is obtained in the required frequency range. This stepped sine method is used in [45] for measuring backbone curves of gongs. Obtaining the backbone estimation using this technique is technically simple but the whole procedure is long and tedious, even when it is automated. Moreover, it was reminded in Sec. 2.3 that the amplitude resonance can be distinct from the phase resonance, especially in case of moderate or high damping. Note also that the forced responses obtained with this stepped sine method are sensible to the jump phenomenon. In particular, measuring the stable solutions close to the saddle-node bifurcation is difficult in practice since their basin of attraction is dramatically reduced and some small perturbation of the system can drive it to the coexisting low amplitude response. In practice a small frequency step should be used as well as perfectly continuous excitation. In the following, this method will be referred as Stepped Sine Testing (SST).

A better estimation of the backbone curve can be obtained by the Nonlinear Resonant Decay Method [42] (NLRD), consisting in two steps. In the first one, the system is set at phase resonance for a given mode using force appropriation techniques; in the second step, the excitation is shut down and the system's free oscillations are measured. The estimation of the instantaneous amplitude and frequency, for instance with the help of the Hilbert transform or a Fourier or wavelet transform, allows one to obtain the backbone curve, which is the same as the locus of the phase resonance. This method has been applied to numerous cases for nonlinear identifications [46, 47, 48]. A minor drawback is that the final result of this method relies on the accuracy of the algorithm estimating the instantaneous frequency. Moreover, since we observe the resonance decay, this method leads to measure the nonlinear mode of the damped system and not the one of the underlying conservative one. They are theoretically distinct, but very close if the damping is small. In the experimental part of this work, the PLL method described hereafter will be used to initially set the system in phase resonance.

A third strategy consists in using experimental continuation techniques. Two distinct techniques can be cited. The first one, which is used hereafter in the present study, consists in tracking the backbone curve by locking the system at the phase resonance using a Phase-Locked-Loop (PLL), as it was recently done by Mojrzisch [18] and Peter [49, 19] in this context. Phase control in the context of nonlinear vibrations seems to have been used firstly by Sokolov & Babitsky [50], who aimed to maintain a self-excited system at resonance or exploring its frequency-amplitude relation. They take advantage of the monotonous behaviour of the frequency-phase curves for a limited set of non linear systems. An extension of this method is used by Mojrzisch *et al.* [51, 18] for measuring forced responses around resonance by sweeping the phase between excitation and vibration. The use of the PLL in this context proves to be robust and efficient. Peter *et al.* [19] use a similar design in order to track backbone curves of nonlinear systems. However, no nonlinear identification is made consequently to the experimental results. The obvious advantage of the PLL method over the resonant decay method is that it directly yields the instantaneous frequency and amplitude, thus avoiding the use of a Fourier or wavelet transform. However the technique may have several drawbacks, especially when the phase is not monotonous, for instance when internal resonances are involved [49]. This technique is used in this paper for the experimental characterization of nonlinear systems and is thoroughly described in Sec. 3.

The second continuation technique is the so-called control-based continuation, introduced in [52] and developed in a large series of works since (see [53, 54, 55] and reference therein). It combines a stabilizing feedback control and a path-following technique as a function of an arclenth parameter, as in numerical continuation methods. This technique share with the PLL method the same stabilizing and non intrusive property: unstable periodic solutions of the system are stabilized but not changed. However, it is more general than the PLL since it relies on an arclenth parametrization of the path and is thus able to tackle any saddle-node (fold) bifurcation, but it requires more experimental efforts. In contrary, the PLL method used here relies on a prescribed phase

and is able to follow a path only if the phase is monotonous along this path. This property is verified for dynamics that involve only one nonlinear mode (the present article give examples in the case of systems with geometrical nonlinearities). On the contrary, this can be a restriction if the dynamics is based on more than one nonlinear mode, and especially when internal resonance occur, since in this case, the phase can be no more monotonous and some pitchfork bifurcations occur (see [20, 56, 49] for systems with 1:1, 1:2 and 1:3 internal resonances).

3 Phase-locked loop controller

3.1 Design

We consider a mechanical vibratory system of displacement (output) response $x(t)$ driven by an input force $F(t)$. The principle behind the phase-locked loop is to adjust the frequency Ω of a harmonic excitation signal so that a prescribed phase lag φ_c is imposed between the measured force signal $F_{\text{meas}}(t)$ of the tested system and its response $x(t)$. Basically, the PLL is composed of a phase detector, a controller and a voltage-controlled oscillator (VCO) (see Fig. 3(a)), as described in Refs. [57, 18, 49, 19]. The phase detector gives an estimation $\hat{\varphi}$ of the actual phase lag φ between the excitation and response signals; the difference e between the output $\hat{\varphi}$ of the phase detector and the command φ_c is fed to an integral controller with gain K_I. The controller yields a correction y to an initial prescribed frequency ω_{ini}. The result Ω feeds the VCO exciting the nonlinear system to be controlled, with amplitude F. The PLL then automatically adjusts the frequency to obtain the intended phase lag.

Ref. [57] details the different possibilities for the practical realization of the phase detector. In our case, the phase and the amplitude of the first harmonic of both x and F_{meas} are detected using a synchronous demodulation (also known as homodyne detection and used in lock-in amplifiers [58]). By multiplying a signal by $\cos\Omega t$ and $\sin\Omega t$ and low-pass filtering the result, one is indeed able to recover the amplitude and phase of the component at Ω contained in the signal (see Fig. 3(b)). This implementation of the phase detector is then interesting because it gives a robust estimation of amplitude and phase of a given harmonic contained in a signal. This estimation is especially more robust than the one obtained with a Fourier transform. This is useful for several reasons: first, it yields an estimation of the amplitude of first harmonic of the displacement (i.e. giving the backbone curve). Second, one can also obtain an estimation of the amplitude of the first harmonic of the injected force, in order to apply a control on it. Finally, a robust estimation of the phase of the first harmonic of both displacement and injected force yields a direct estimation of the phase lag, leading to an amplitude independent error signal e and giving the possibility to use an arbitrary phase command, contrary to simpler designs of phase detector [59, 57].

Two different measurements are possible using this PLL design:

— By setting the phase command φ_c at $\pi/2$ (phase resonance) and varying the excitation amplitude F, the backbone can be recorded by measuring the amplitude of the first harmonic of x.

— Conversely, the PLL can also be used to measure the forced responses around resonance, even if it is unstable in open loop, by sweeping the phase φ_c over the range $[0, -\pi]$ while keeping the injected force excitation F_{meas} constant.

3.2 Stability

We consider a mechanical systems whose behaviour is modelled by a the single Duffing oscillator of Eq. (17). We investigate in this section its stability when driven by a PLL controller described in the previous section. The stability of this controlled Duffing oscillator has already been studied by Fan [59] in the case of $\varphi_c = \pi/2$, that is when the PLL locks it in phase resonance. A slight difference with [59] lies however in the implementation of the phase detector. The multiplying phase detector used in [59] (*i.e.* consisting in lowpass filtering the product of measured and excitation signals) only allows to obtain phase quadrature. In the following, we extend these results to any value of the phase command φ_c, which is made possible by a direct phase lag estimation provided by the synchronous demodulation.

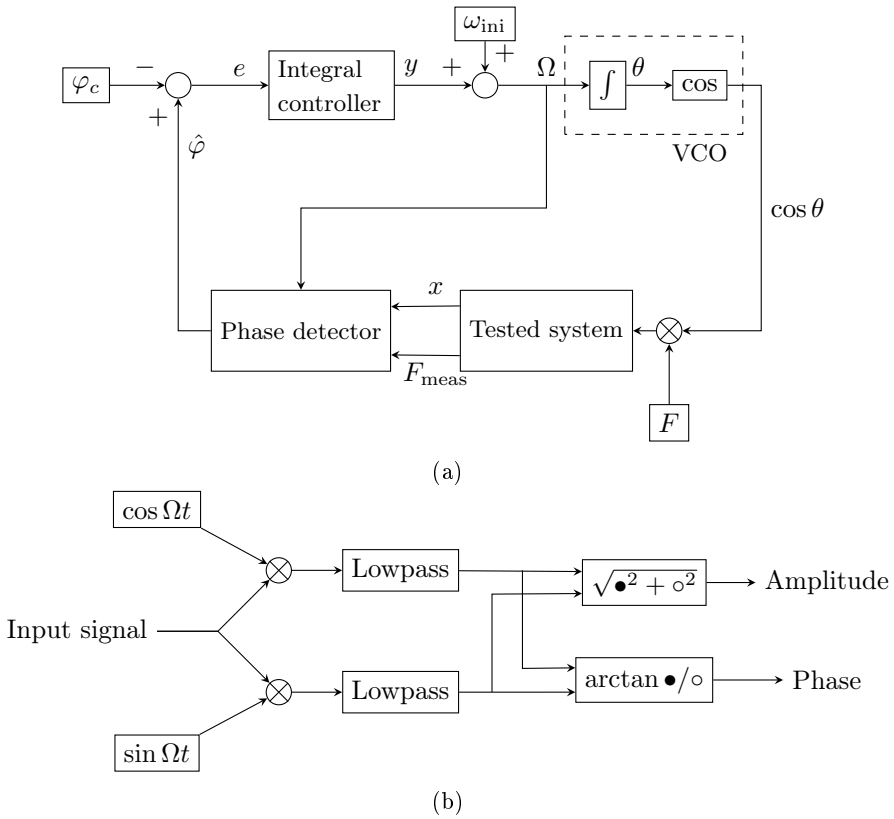

Figure 3 – (a) Scheme of the PLL. F and φ_c are the commands. (b) Implementation of the synchronous demodulation used in the phase detector.

We consider the nonlinear phase-controlled system:

$$\begin{cases} \ddot{x} + 2\xi\omega_0\dot{x} + \omega_0^2 x + \hat{\Gamma}_0 x^3 = F\cos\theta, & \text{(28a)} \\ \dot{\theta} = \omega_{\text{ini}} + y, & \text{(28b)} \\ \dot{y} = K_I e, & \text{(28c)} \\ e = (\hat{\varphi} - \varphi_c), & \text{(28d)} \\ \dot{\hat{\varphi}} = \omega_c(\varphi - \hat{\varphi}), & \text{(28e)} \end{cases}$$

where x is the system's response, ω_0 its natural angular frequency, ξ its damping factor, $\hat{\Gamma}_0$ its cubic nonlinearity parameter and F the amplitude of the harmonic forcing. $\dot{\theta} = \Omega$ denotes the frequency of the VCO, φ is the actual phase lag between response $x(t)$ and excitation (see Eq. (29a)), $\hat{\varphi}$ is the output of the phase detector and the estimation of φ, K_I is the integral gain of the controller, y is the output of the controller. We assume here that the phase detector has a small delay and that it behaves as a perfect sensor with a first order low-pass filter of cut-off frequency ω_c. In practice, higher order filters are used and the following developments are still valid for fast enough low pass filters.

The system is solved by an averaging method [60]. We rewrite (28) at first order by letting $x_1 = x$ and $x_2 = \dot{x}$. A solution is then sought with the following form:

$$\begin{cases} x_1 = a\cos(\theta + \varphi), & \text{(29a)} \\ x_2 = -a\omega_0\sin(\theta + \varphi). & \text{(29b)} \end{cases}$$

Substituting Eqs. (29) in Eqs. (28), we obtain the following formulation in terms of amplitude and phase angle:

$$\begin{cases} \dot{a} = \dfrac{-1}{\omega_0}\left[2\xi\omega_0^2 a\sin(\theta+\varphi) - \hat{\Gamma}_0 a^3\cos^3(\theta+\varphi) + F\cos\theta\right]\sin(\theta+\varphi), & \text{(30a)} \\ \dot{\varphi} = -y + \omega_0 - \omega_{\text{ini}} - \dfrac{1}{a\omega_0}\left[2\xi\omega_0^2 a\sin(\theta+\varphi) - \hat{\Gamma}_0 a^3\cos(\theta+\varphi)^3 + F\cos\theta\right]\cos(\theta+\varphi), & \text{(30b)} \\ \dot{y} = K_I(\hat{\varphi} - \varphi_c), & \text{(30c)} \\ \dot{\hat{\varphi}} = \omega_c(\varphi - \hat{\varphi}), & \text{(30d)} \\ \dot{\theta} = \omega_{\text{ini}} + y. & \text{(30e)} \end{cases}$$

In the averaging method, it is assumed that the time dependent variables a, $\hat{\varphi}$, y and ϕ, there first time derivatives and $\dot{\theta} = \Omega$ vary at a slow time scale with respect to the periodic fast time scale. Averaging over a period (*i.e.* applying $\frac{1}{2\pi}\int_0^{2\pi} \mathrm{d}\theta$ to the equations), we obtain the simplified equations:

$$\begin{cases} \dot{a} = -\xi\omega_0 a - \dfrac{F}{2\omega_0}\sin\varphi, & \text{(31a)} \\ \dot{\varphi} = -y + \omega_0 - \omega_{\text{ini}} + \dfrac{3\hat{\Gamma}_0}{8\omega_0}a^2 - \dfrac{F\cos\varphi}{2a\omega_0}, & \text{(31b)} \\ \dot{y} = K_I(\hat{\varphi} - \varphi_c), & \text{(31c)} \\ \dot{\hat{\varphi}} = \omega_c(\varphi - \hat{\varphi}), & \text{(31d)} \\ \Omega = \omega_{\text{ini}} + y, & \text{(31e)} \end{cases}$$

where the frequency $\Omega = \dot{\theta}$ becomes an additional variable. The Duffing oscillator in open-loop can be recovered by setting $y(t) = 0$, which implies that $\omega_{\text{ini}} = \Omega$ is the prescribed excitation frequency.

Now, the fixed points $(a_s, \varphi_s, \hat{\varphi}_s, y_s, \Omega_s)$ are sought by imposing $\dot{a} = \dot{\varphi} = \dot{y} = \dot{\hat{\varphi}} = 0$. At first, one obtains $\varphi_s = \hat{\varphi}_s = \varphi_c$: the actual and estimated phase of $x(t)$ with respect to the forcing are equal to the command value φ_c. Moreover, the amplitude and phase of $x(t)$ in the steady state are:

$$\begin{cases} a_s = \dfrac{-F}{2\xi\omega_0^2}\sin\varphi_c, & \text{(32a)} \\ \Omega_s = \omega_0 + \dfrac{3\hat{\Gamma}_0 F^2}{32\xi^2\omega_0^5}\sin^2\varphi_c + \dfrac{\xi\omega_0}{\tan\varphi_c}, & \text{(32b)} \end{cases}$$

with the following correction to the initial frequency:

$$y_s = \omega_0 - \omega_{\text{ini}} + \frac{3\hat{\Gamma}_0 F^2}{32\xi^2\omega_0^5}\sin^2\varphi_c + \frac{\xi\omega_0}{\tan\varphi_c}. \quad (33)$$

The fixed points defined by Eqs. (32) are those of a classical Duffing oscillator: the closed loop steady state response is the same than the open loop one. As a conclusion, the above results show that the system's behaves as if it was in open-loop, with its phase imposed by the PLL to its prescribed value φ_c.

The stability of the fixed point is studied by writing the jacobian matrix $\boldsymbol{J}$ of (31a-d):

$$\boldsymbol{J} = \begin{bmatrix} -\xi\omega_0 & \frac{-F}{2\omega_0}\cos\varphi & 0 & 0 \\ \frac{3\hat{\Gamma}_0}{4\omega_0}a + \frac{F\cos\varphi}{2\omega_0 a^2} & \frac{F\sin\varphi}{2a\omega_0} & 0 & -1 \\ 0 & \omega_c & -\omega_c & 0 \\ 0 & 0 & K_I & 0 \end{bmatrix}, \quad (34)$$

and evaluating it at the fixed point using (32a):

$$\boldsymbol{J}_s = \begin{bmatrix} -\xi\omega_0 & \frac{-F}{2\omega_0}\cos\varphi_c & 0 & 0 \\ \frac{-3\hat{\Gamma}_0 F}{8\xi\omega_0^3}\sin\varphi_c + \frac{2\xi^2\omega_0^3\cos\varphi_c}{F\sin^2\varphi_c} & -\xi\omega_0 & 0 & -1 \\ 0 & \omega_c & -\omega_c & 0 \\ 0 & 0 & K_I & 0 \end{bmatrix}. \quad (35)$$

The system is stable if the real parts of the eigenvalues of $\boldsymbol{J}_s$ are strictly negative. We first consider the top

left 2×2 part of the jacobian matrix (35) that concerns the Duffing oscillator (19) in open-loop. By computing the eigenvalues λ and ensuring they have a strictly negative real part, one can derive the stability criterion:

$$G < \xi^2\omega_0^2, \tag{36}$$

where G is a function of F and φ_c:

$$G = \frac{3\hat{\Gamma}_0 F^2}{16\xi\omega_0^4}\cos\varphi_c \sin\varphi_c - \frac{\xi^2\omega_0^2}{\tan{\varphi_c}^2}. \tag{37}$$

By eliminating F between Eqs. (37) and (32a,b), one obtains two conditions equivalent to an instability region in the $(a_s, \varphi_s, \Omega_s)$ space, shown in grey on Fig. 2, that is independent of F. Its limit can be plotted by computing a_s and Ω_s as a function of φ_s and varying it. The unstable part of a given open-loop frequency response is consequently obtained by its intersection with the instability region, the limits being obtained at the two saddle-node bifurcations points. This instability region is also shown in light red in Fig. 4(a), for parameters $\omega_0 = 1$, $\Gamma_0 = 1$, $\xi = 1 \times 10^{-2}$. For a frequency response with $F = 6 \times 10^{-3}$, an unstable part is found, whereas for $F = 3 \times 10^{-3}$, the whole frequency response is stable.

We consider now the closed-loop system. The particular case $\varphi_c = \pi/2$ is already treated in [59], with a different phase detector. Writing the determinant $\det(\boldsymbol{J}_s - \lambda\boldsymbol{I})$ and applying the Routh-Hurwitz criterion, the following stability criterion is obtained:

$$K_I < (\xi\omega_0 + \omega_c)\xi\omega_0. \tag{38}$$

In the general case $\varphi_c \neq \pi/2$, the stability condition is more complex and the determinant writes

$$\begin{aligned}\det(\boldsymbol{J}_s - \lambda\boldsymbol{I}) &= \xi\omega_0\omega_c K_I + \lambda\omega_c(K_I + \xi^2\omega_0^2 - G) + \lambda^2(2\xi\omega_0\omega_c + \xi^2\omega_0^2 - G) + \lambda^3(2\xi\omega_0 + \omega_c) + \lambda^4 &(39)\\ &= \alpha_0 + \alpha_1\lambda + \alpha_2\lambda^2 + \alpha_3\lambda^3 + \lambda^4. &(40)\end{aligned}$$

Using the Routh-Hurwitz criterion, one shows that the system is stable if:

$$\alpha_i > 0, \tag{41}$$

$$\alpha_3\alpha_2\alpha_1 > \alpha_1^2 + \alpha_3^2\alpha_0, \tag{42}$$

$$\alpha_3\alpha_2 > \alpha_1, \tag{43}$$

which translates in

$$\xi\omega_0\omega_c K_I > 0, \tag{44a}$$

$$2\xi\omega_0 + \omega_c > 0, \tag{44b}$$

$$G < 2\xi\omega_0\omega_c + \xi^2\omega_0^2, \tag{44c}$$

$$G < K_I + \xi^2\omega_0^2, \tag{44d}$$

$$\omega_c K < 4\xi^2\omega_0^2\omega_c + 2\xi^3\omega_0^3 + 2\xi\omega_0\omega_c^2 - 2\xi\omega_0 G, \tag{44e}$$

$$\begin{aligned}&\omega_c K_I^2 + K_I(2\xi^3\omega_0^3 + \xi^2\omega_0^2\omega_c - \xi\omega_0\omega_c^2 - (\omega_c - 2\xi\omega_0)G)\\ &- \left[4\xi^4\omega_0^4\omega_c + 2\xi^3\omega_0^3\omega_c^2 + 2\xi^5\omega_0^5 - (4\xi^3\omega_0^3 + 4\xi^2\omega_0^2\omega_c + 2\xi\omega_0\omega_c^2)G + 2\xi\omega_0 G^2\right] < 0.\end{aligned} \tag{44f}$$

Criteria (44a) and (44b) are naturally verified. Criterion (44c) limits the choice of ω_c and states that the phase detector must be sufficiently fast. The gain K_I is chosen using criteria (44d, 44e, 44f). Note that (44f) does not always allows stability to be found. Only a strictly positive determinant (depending on G) permits to find two separate roots and the region between them where the criterion is verified. Overall, from criteria (44a-44f), stability may involve the *a priori* knowledge of the nonlinearity.

Following the same procedure than for the open-loop case, an instability region is found for the PLL-driven oscillator, derived from criteria (44a-44f) along with Eqs. (37) and (32a,b) in which F has been eliminated. For any value of φ_c, the strictest criterion ensuring stability is found numerically and translated in a (a_s, Ω_s) pair. Instability regions obtained for ω_c=0.2 (so that $\omega_c \ll \omega_0$ and criterion 44c is respected) and several values of the integral gain $K_I = 2 \times 10^{-4}$, 4.7×10^{-4} and 1×10^{-3} are plotted on Fig. 4(a). One can observe that the effect of the gain K_I is to move the instability region toward the high frequencies / amplitudes, which explains its stabilizing effect. Consequently, a given frequency response can be partially unstable (blue area) or stable (green and orange areas) depending on the gain and the position of the instability region. For any given excitation amplitude, there exists a limit value $K_I^{\lim}$ of the gain K_I for which the frequency response becomes fully stable. For $F = 6 \times 10^{-3}$, $K_I^{\lim} = 10^{-3}$ since the green instability region is tangent to the frequency response of the

oscillator.

The dependence of the limit gain K_I^{lim} on the forcing amplitude F is plotted on Fig. 4(b) using criteria (44a-44f) and Eq. (37). The curves are dependent on both the damping ξ in the system and the cut-off frequency of the low pass filter ω_c, corresponding to the speed of the phase detector. The bigger ω_c, the better the system can be controlled since the maximum amplitude that can be reached is higher. Also, when K_I tends to 0, the closed-loop maximum amplitude tends to a constant that is the maximum amplitude for the open-loop system to be stable; it can be retrieved by looking at criterion (44d) but it is also suggested by Fig. 4(a).

In Fig. 4(b), the reversed bell shape of the curves informs us that very good performance, *i.e.* a high excitation amplitude, can be reached at the cost of a precise adjustment of the controller: one can increase K_I only up to a point from which an increase will only worsen stability properties. However, there was no need for such performance in our experiment, especially if one is interested only in backbone curves; it was therefore relatively easy to find empirically a correct K_I.

In practice, a small proportional gain can be added to the controller for increasing the speed of the PLL without increasing the sensibility to noise. For the experimental implementation, a higher order filter (fourth order Butterworth filter) is also used in the phase detectors. This does not fundamentally change the stability properties: as shown in Fig. 4(b), the cut-off frequency ω_c has an influence on the instability region of the PLL-driven system but as long as the filter, *i.e.* the phase detector, is fast enough, stability is ensured on the whole phase domain. Note that a first order filter is sufficient for the experimental PLL to function but was found to yield noisier results in tested cases.

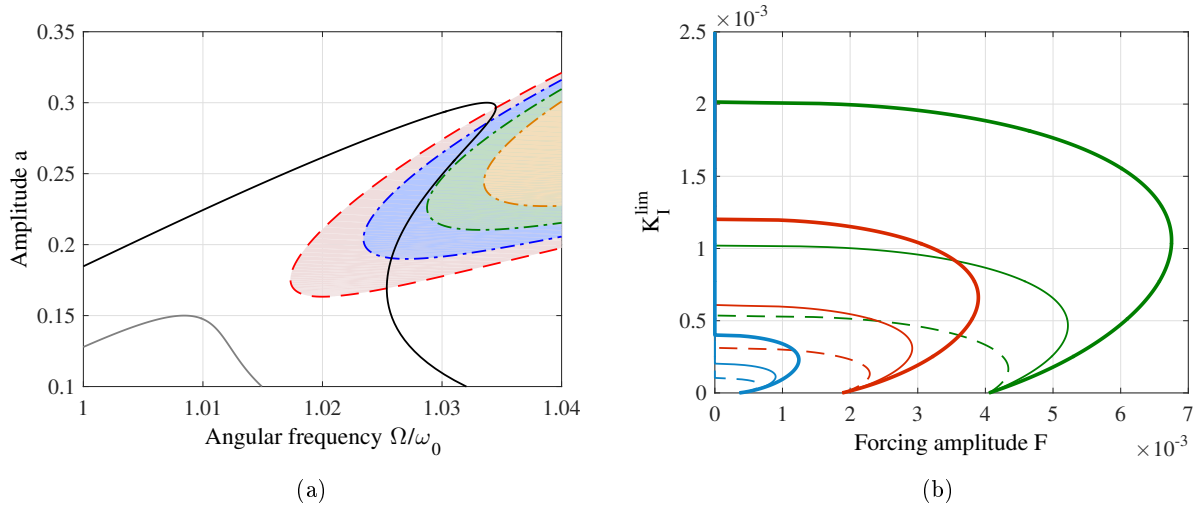

(a) (b)

Figure 4 – (a) Frequency response of Duffing oscillator for $F = 6 \times 10^{-3}$ (black solid line) and $F = 3 \times 10^{-3}$ (solid gray line) and instability regions in open-loop (red dashed line / light red area), for $K_I = 0.2 \times 10^{-4}$ (blue dashed-dotted line / light blue area), for $K_I = 4.7 \times 10^{-4}$ (green dash-dotted line / light green area) and for $K_I = 1 \times 10^{-3}$ (orange dash-dotted line / light orange area). (b) Limit gain K_I^{lim} for stability depending on forcing F for several configurations: $\xi = 0.002$ (blue), $\xi = 0.006$ (red), $\xi = 0.01$ (green) and ω_c=0.05 (dashed line), 0.1 (thin solid line), 0.2 (thick solid line) rad.s^{-1}.

3.3 Numerical validation

In Fig. 5(a), the results of a MATLAB/Simulink simulation of a PLL-driven Duffing oscillator are compared with the numerical solutions using the HBM/ANM method with the software Manlab for numerical continuation [40]. The parameters used are close to those of an experimental system ($\omega_0 = 394.9610$ rad.s^{-1}, $\hat{\Gamma}_0 = 5.1054 \times 10^5$ s^{-2}, $\xi = 5 \times 10^{-4}$). The PLL was set with a starting frequency of 392 rad.s^{-1}, an integral gain of 10, a proportional gain of 0.5. The forcing starts at F=1 s^{-2} for the backbone curve while it is maintained at F=10 s^{-2} for the frequency response. It is noticeable that the backbone obtained with the PLL in forced regime is identical to the numerical solution in free regime. Moreover, when the phase is swept for a given amplitude of excitation, we see that the PLL is able to drive the system to the correct frequency and that we are able to recover the numerical solution, including in the unstable region which is stabilized by the PLL. Both the backbone curve and the frequency response are preceded by a short transient regime, shown here for the sake of completeness, during which the PLL is self-adjusting: the frequency oscillates and the amplitude of

vibration varies accordingly. In Fig. 5(b), one can check the precision and the speed of the phase detector: the delay is indeed very small between signal x and its first harmonic reconstructed using the outputs of the phase detector.

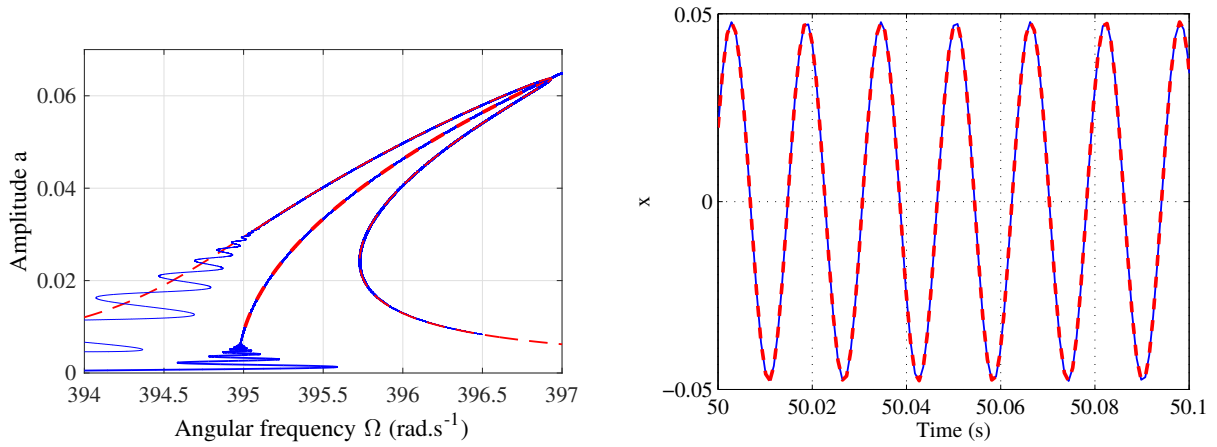

(a) (b)

Figure 5 – (a) Comparison of the simulated response of the PLL-driven Duffing oscillator and the numerical Manlab solution: forced response by Manlab (dashed red line) and PLL (solid blue line), backbone curve by Manlab (thick dashed red line) (free) and by PLL (thick solid blue line) (forced). φ_c varies between $\pi/6$ and $11\pi/12$ rad. (b) Comparison of the motion x the PLL-driven Duffing oscillator (solid blue line) and first harmonic found using the phase detector (dashed red line).

4 Experiments

4.1 Setup

The proposed nonlinear identification method is applied to three different structures. The first one is a circular plate, identical to the one studied in [61, 20]. The second structure is a chinese gong on which two modes are identified. The third structure is a piezoelectric unimorph cantilever beam, that can be used for energy harvesting purpose. In this case, the nonlinear mode identification is done in the open and short-circuit configuration of the piezoelectric patch. The plate, the gong and the beam are represented in Figs. 6(a,b,c).

The chinese gong and the circular plate are excited by a non contact coil / magnet apparatus, already described and used in [20]. According to [42, 46], it is complex to qualify a priori the relation between the spatial distribution of the excitation force and the accuracy of the NNM isolation. Ref. [46] also mentions that a single point mono-harmonic excitation may be sufficient for satisfactory NNM isolation. In the meantime, according to Eq. (11) for small amplitude at first order, the motion onto one NNM is synchronous monoharmonic and has the shape of the i-th mode; hence, the magnet can be placed anywhere (except on a node) and is placed closed to an antinode of vibration of the mode to be identified in order to minimize the excitation force. The force is directly proportional to the current in the coil and can thus be measured using the current monitoring output of the amplifier (B&K 2712). The piezoelectric beam is base-excited by an electromagnetic shaker (B&K 4808) and a power amplifier (B&K 2712). The base acceleration and the beam velocity are measured using an accelerometer (PCB 352C65) and a laser vibrometer (Polytec PSV-400). The velocity is measured at an arbitrary point close to the free extremity of the beam.

The setup is driven by a dSPACE MicroLabBox on which is implemented the control scheme using Matlab/Simulink. The sampling frequency is set to 50 kHz. This high frequency was chosen because it corresponds to a small time step necessary for the accuracy of the numerical scheme and it avoids the presence of high frequencies in the output synthesized by the dSPACE. The filter used in the phase detector has a cut-off frequency of 20 Hz. A picture of the setup is displayed in Fig. 6(d). For the sake of completeness, it should be mentioned that when the vibration exciter is an electromagnetic shaker, a second controller is used to correct F, avoiding force drops off near resonance [62] and maintaining the amplitude of injected force constant. It is verified *a posteriori* that this second closed-loop control is not needed in the case of the coil-magnet excitation.

In addition to the PLL measurement, two other measurement methods are used in order to validate the experimental procedure. The forced responses around resonance are measured with a stepped sine sweep excitation, as described in Sec. 2.4. A National Instrument acquisition card (NI-PXI 6229) is used for that matter, controlled by MATLAB in which the stepped sine in programmed. The NLRD method [42, 46] is also used. Since the system is driven in phase quadrature, assuming that the phase quadrature of the first harmonic is sufficient, the NNM resonant decay should yield the free amplitude-frequency relationship when the excitation initiated with the PLL is turned off. On a side note, the PLL method could be implemented such as it verify the force appropriation criterion [42] considering several harmonics. In fact, the recent work by Peter [19] proposes a criterion using the higher harmonics to check a posteriori the correct isolation of the NNM, even if the phase resonance testing is implemented with a single harmonic. In the current experiments, it has been observed that the harmonic distortion in both the excitation force and the response was relatively weak. Quantifying the influence of higher harmonics is beyond the scope of the present article but discussions on this topic can be found in [19].

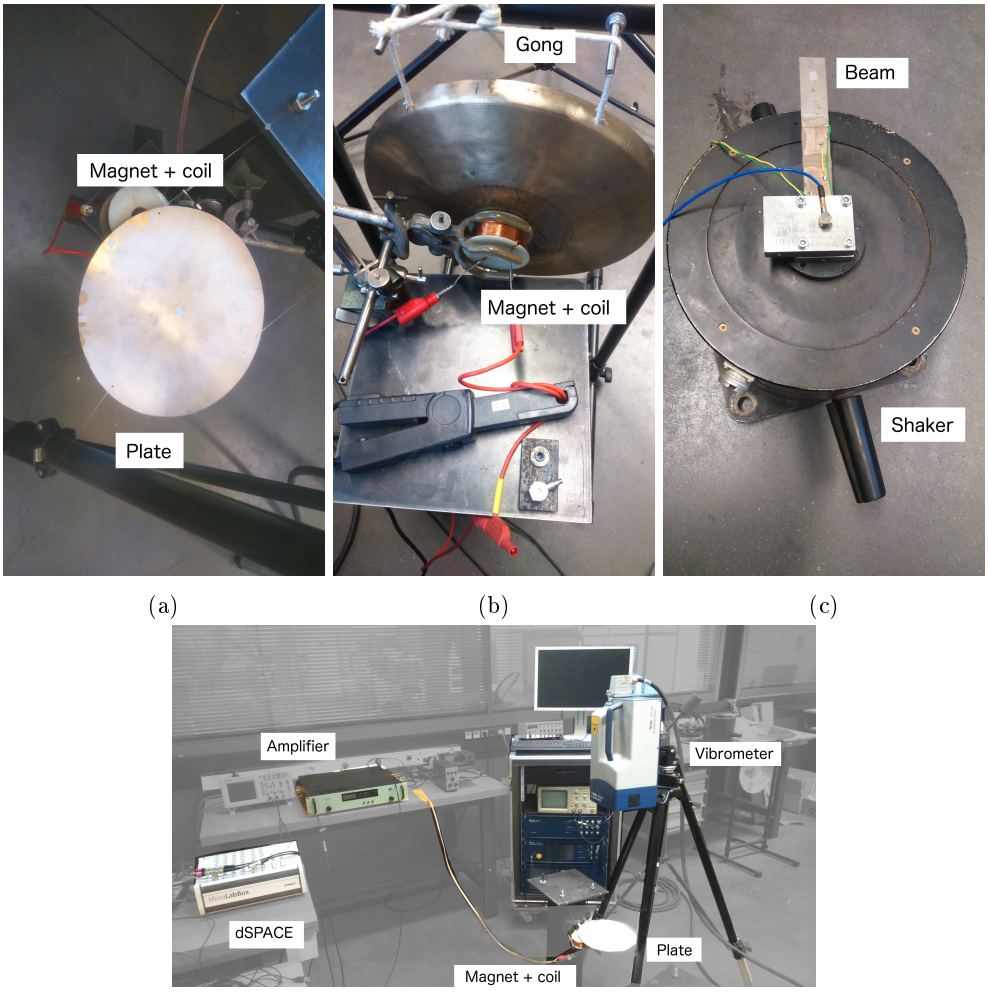

(a) (b) (c)

(d)

Figure 6 – Experimental setup : (a) Circular plate, (b) gong and coil, (c) piezoelectric beam, shaker and accelerometer, (d) Plate, magnet and coil apparatus, vibrometer, amplifier and dSPACE MicroLabBox.

4.2 Axisymmetric and asymmetric modes of a circular plate

The plate is made of brass, has a radius of 110 mm and a thickness of 1.6 mm. It is set-up horizontally, maintained with three thin wires. The first axisymmetric mode and the first asymmetric mode of the circular plate are considered. The operational deflection shapes displayed in Fig. 7 are recovered from a modal analysis done with the scanning laser vibrometer. The two asymmetric companion modes (2,0) have slightly different frequencies, due to unavoidable imperfections. The mode with the lowest frequency is referred as mode (2,0,1) and the one with the highest as mode (2,0,2). The effect of the mistuning of these two companion modes on

the forced response have thoroughly been studied in [61, 20]. In these measurements on the circular plate, the integral gain of the PLL is set to 15, with a proportional gain of 0.5. Since the plate response is measured by the laser vibrometer (which measures the velocity), we impose a zero phase lag between forcing and velocity for the measurement of a backbone curve. Force responses measurement are obtained by varying the phase between $-\pi/3$ and 1.2 rad, with a sweep rate of 0.015 rad.s^{-1}.

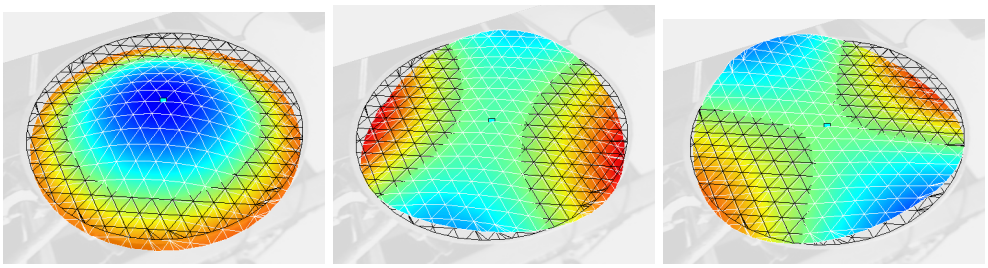

(a) (b) (c)

Figure 7 – Operational shapes of the plate at frequencies of (a) the axisymmetric mode (0,1) (194 Hz) and the asymmetric companion modes (b) (2,0,1) (105 Hz) and (c) (2,0,2) (111 Hz)

Figs. 8(a,b) displays the backbone curves obtained using the PLL. They also show several forced responses in amplitude and phase of the displacement for different excitation levels. The unstable region of the forced response is stabilized and can be measured, even for high amplitudes. The backbone passes very close to the maximum of amplitude for each forced responses, as it is described in Sec. 2.

It is straightforward to fit a parabola (least-square with constant and quadratic coefficients) on the backbone obtained using the PLL (see Fig. 8(c)). The backbone obtained using the NLRD method and the corresponding fitted parabola are also plotted on Fig. 8(c). In this case the instantaneous frequency and amplitudes are recovered by taking the ridge of the Short-Time-Fourier-Transform of the decaying signal.

From the fitted parabolas, one can extract the nonlinear cubic coefficient $\hat{\Gamma}_0$ and the linear frequency $f_0 = \omega_0/2\pi$ appearing in Eq. (28a); Note that if x is the displacement, $\hat{\Gamma}_0$ in Eq. (28a) is easily related to Γ_0 of the NNM appearing in Eq. (17) with the help of Eq. (11):

$$\Gamma_0 = \hat{\Gamma}_0 \Phi_m^2, \tag{45}$$

where Φ_m is the value of the modal shape at the measurement point (obtained theoretically or experimentally). The parameters f_0 and $\hat{\Gamma}_0$ are presented in Tab. 1 for the two methods. The identified coefficients and frequencies are identical, which cross-validates the techniques

The backbones curves of the two asymmetric companion modes (2,0,1) and (2,0,2) are plotted on Fig. 9. For mode (2,0,1), a change of curvature can be observed around 112 Hz. This is due to a 1:1 internal resonance with mode (2,0,2) being activated, leading to a bifurcation towards a coupled solution [20, 63]. Hence, it is proposed to identify the nonlinear mode using the first region of the backbone only. The parabolas fit very well from 105 to 112 Hz, and the estimation differs when the coupled solution appears. In the case of mode (2,0,2), the internal resonance does not seem to be activated and the identification can be made on the whole backbone curve. Furthermore, one can notice that the results obtained with the phase resonance and the resonant decay methods are identical. The identified parameters are presented in Tab. 1.

Finally, the experimentally identified frequencies and coefficients can be compared to those obtained with a nonlinear model of the circular plate. For this matter, the dimensionless frequency and cubic coefficient are found following the methodology presented in Appendix A. The obtained dimensionless coefficients for a generic circular plate given by the model of [61] are referenced in Tab. 1. It appears that the frequencies $\bar{\omega}$ are very well estimated by the model and that small differences are observed for the $\bar{\Gamma}$ coefficients.

It is quite remarkable that the parabola fits so well the measured backbone for modes (0,1) and (2,0), even for high amplitudes: for the asymmetric modes (2,0), the highest vibration amplitude reaches the thickness of the plate. This fact means that the first order approximation made in Sec. 2 still applies and that higher effects play a negligible role. It fully justifies the proposed approach.

4.3 Axisymmetric and asymmetric modes of a Chinese Gong

Chinese gongs display an important pitch glide in playing situations. The pitch glide direction can be related to the hardening / softening behaviour of a NNM; It depends on the central section geometry and

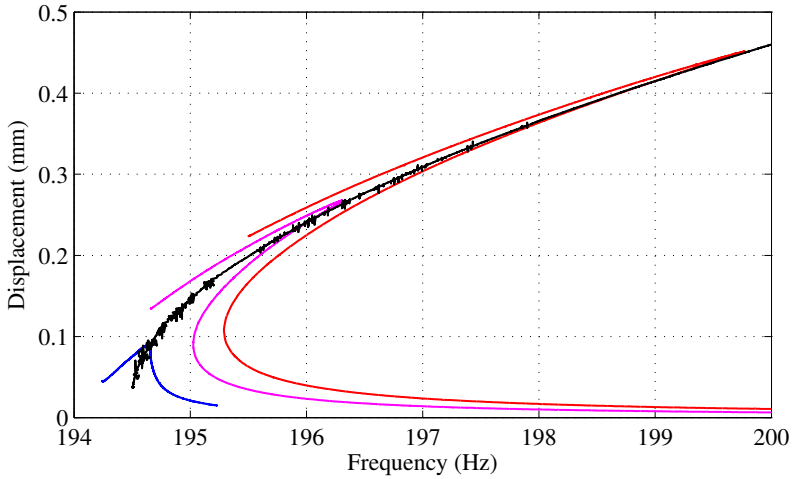

(a)

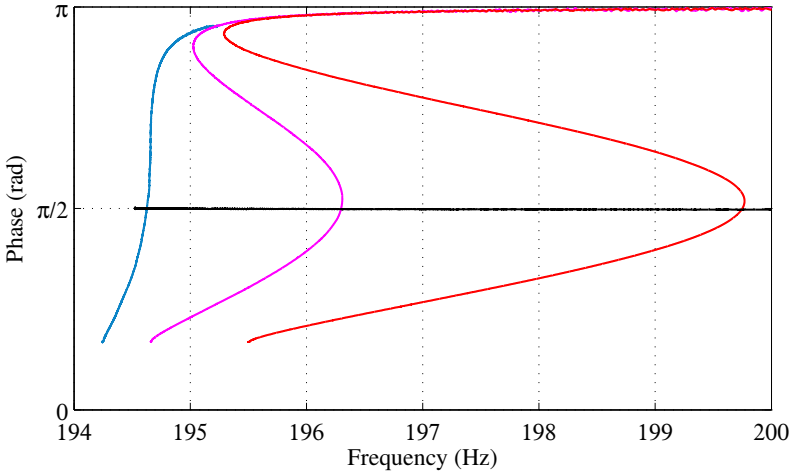

(b)

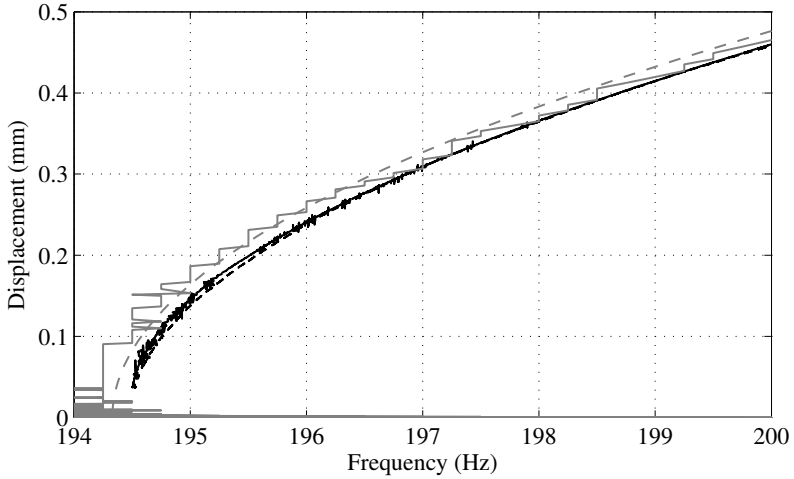

(c)

Figure 8 – Mode (0,1) of the circular plate : backbone curve obtained using the PLL (black) and forced responses measured with PLL under currents 0.48 (blue), 1.42 (purple) and 2.38 A (red): amplitude (a) and phase (b). (c) Backbone curves obtained using the PLL, fitted parabola (dashed black), backbone curve using NLRD (gray), fitted parabola (dashed gray).

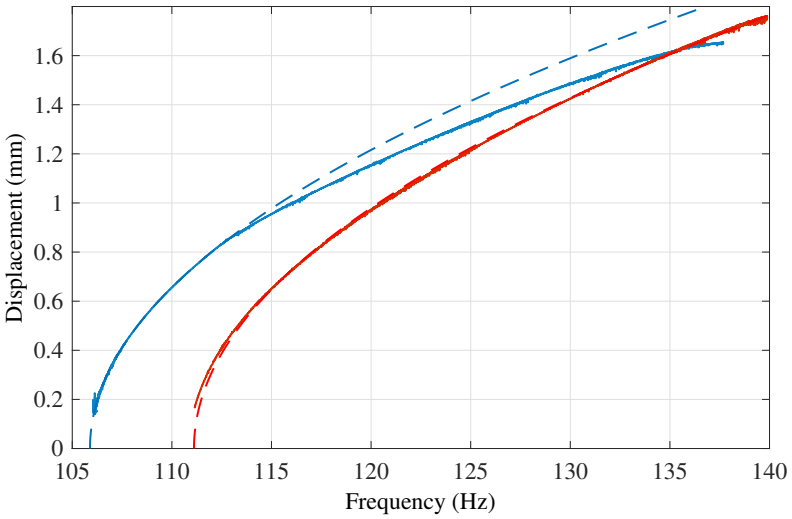

(a)

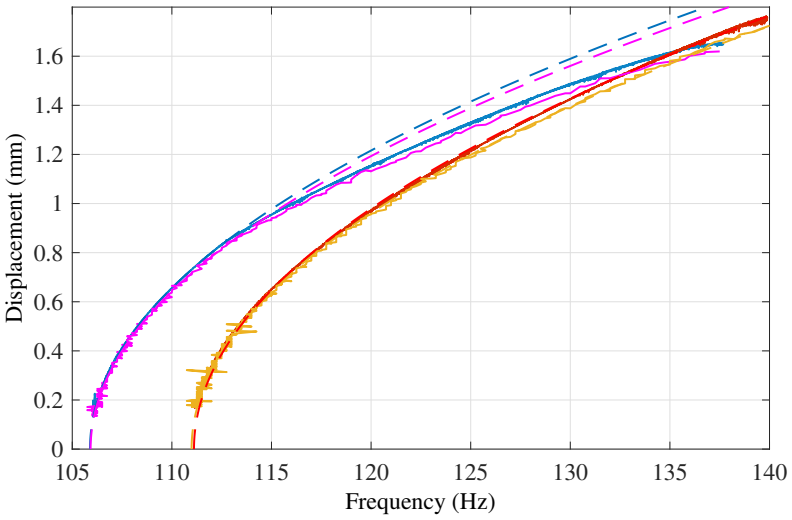

(b)

Figure 9 – Modes (2,0) of the circular plate. (a) backbone curve, obtained with PLL, of mode (2,0,1) (blue) and mode (2,0,2) (red), along with fitted parabolas (dashed curves). (b) Same as (a) with the measurements from the NLRD method added: mode (2,0,1) (magenta) and mode (2,0,2) (orange) along with fitted parabolas (dashed curves)

Mode (0,1)			
	PLL	NLRD	Model
f_0 (Hz)	194.5	194.33	
$\hat{\Gamma}_0$ ($m^{-2}.s^{-2}$)	5.1127×10^{11}	5.1127×10^{11}	
$\bar{\omega}$	9.070	9.062	9.175
$\bar{\Gamma}$	9.126	9.126	8.575
Mode (2,0,1)			
	PLL	NLRD	Model
f_0 (Hz)	105.89	105.92	
$\hat{\Gamma}_0$ ($m^{-2}.s^{-2}$)	1.0639×10^{11}	1.1028×10^{11}	
$\bar{\omega}$	4.897	4.896	5.093
$\bar{\Gamma}$	2.123	2.201	1.898
Mode (2,0,2)			
	PLL	NLRD	Model
f_0 (Hz)	111.11	110.99	
$\hat{\Gamma}_0$ ($m^{-2}.s^{-2}$)	1.0842×10^{11}	1.1400×10^{11}	
$\bar{\omega}$	5.176	5.133	5.093
$\bar{\Gamma}$	2.171	2.270	1.898

Table 1 – Experimentally identified (PLL and NLRD) and theoretical nonlinear coefficients for modes (0,1), (2,0,1) and (2,0,2) of the circular plate.

reduces essentially to the ratio of the central section thickness to curvature [64, 65]: gongs with a flat central area display a downward pitch glide (hardening behaviour) whereas those with a convex central area display an upward pitch glide (softening behaviour). Identifying the nonlinear parameters of the modes involved could help to find links between the sound and the geometrical or material characteristics.

The measured chinese gong has a diameter of 314 mm and a thickness of 1.5 mm approximately. The central area display a flat profile so that a hardening behaviour is expected for the fundamental nonlinear mode [65]. The gong is set-up vertically, in playing conditions. We focus on the first axisymmetric mode (0,1) and the first asymmetric mode (1,1). The modal shapes displayed in Fig. 10 are recovered from a modal analysis done with the scanning laser vibrometer. The linear eigenfrequencies for the first and third mode are 280 and 478 Hz respectively. In the case of mode (0,1) the magnet is placed in the center of the gong and the vibration is measured at the same place; for mode (1,1) the magnet is placed at the upper anti-node and the vibration is measured at the same place. Note that the structure is sensitive to the magnet position; hence the magnet has an influence on the measured nonlinearity. In these measurements, the integral gain is set to 10, with a proportional gain of 2. As with the circular plate (see Sec. 4.2), the phase difference between forcing and velocity is set to 0 for the measurement of a backbone curve while it varies between $-\pi/3$ and 1.2 rad for a forced response, with a sweep rate of 0.015 $rad.s^{-1}$.

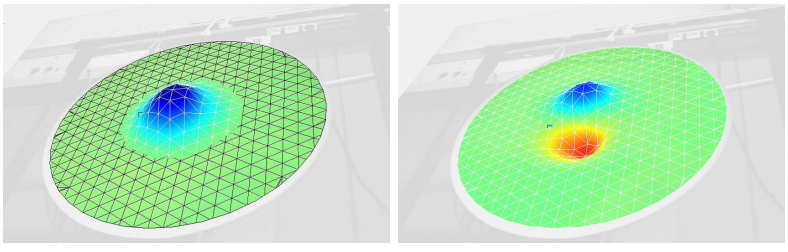

(a) (b)

Figure 10 – Operational shapes of the chinese gong at frequencies of the first axisymetrical mode (0,1) (280 Hz) and asymetrical mode (1,1) (478 Hz).

Fig. 11 displays the backbone curve and the frequency responses around resonance obtained with the PLL measurement method for the first axisymmetric mode (0,1) of the gong. It can be seen that the first mode has a hardening behaviour. Fig. 11 also shows that the frequency response around resonance can be fully recovered including the unstable region for the highest amplitudes. One can notice that at high amplitudes, the backbone curve notably deviates from the top of the frequency response and seems to be in the unstable region. It is likely

due to a slight heating of the coil and magnet excitation system that has consequences on the gong behaviour. It is the main reason the experimental results do not feature higher amplitudes for the gong; this topic should be the subject of a further study. The red curve is noisier than the others in the unstable region. Indeed, approaching the stability limit of the system can enhance noise. Also, since the gong is attached in one point only and positionned vertically, it is very sensitive to any external perturbation, that result in solid body motion for example.

The frequency response measured using SST are also represented on Fig. 11, taking care of reproducing the same excitation levels. This method shows well the jump phenomenon for the highest excitation levels. The two methods give identical results, assessing the validity of the PLL for nonlinear forced responses measurement. For the SST result at the maximum excitation level (yellow triangles), an early jump down may be observed. This is likely to be due to an external perturbation during the experiment. It could be avoided by choosing a very small frequency step. Finally, Fig. 11 shows the backbone curve obtained with the NLRD method and the backbone curve obtained by finding the maxima of amplitude of the frequency responses obtained by SST. Several artefacts can be observed with the NLRD method, due to an insufficient frequency resolution. Finding the instantaneous frequency precisely enough can be a sensible task with this method. Graphically, it is reassuring that the three methods yield sensibly identical results. Note that the estimation of the backbone curve obtained with SST may be incorrect at high amplitude because of the early jump down. More generally since the gong seems to be sensitive to heat, high amplitude excitation can heat it differently depending on the duration of the excitation, possibly leading to discrepancies in the resonance frequency.

For this first mode, the nonlinear identification yields the parameters indicated in Tab. 2 for the three methods. The fitted parabolas are not shown on Fig. 11 for readability concerns. The nonlinear cubic coefficients $\hat{\Gamma}_0$ obtained with the three methods display small discrepancies but it may be due to the quality of the results obtained with NLRD and SST.

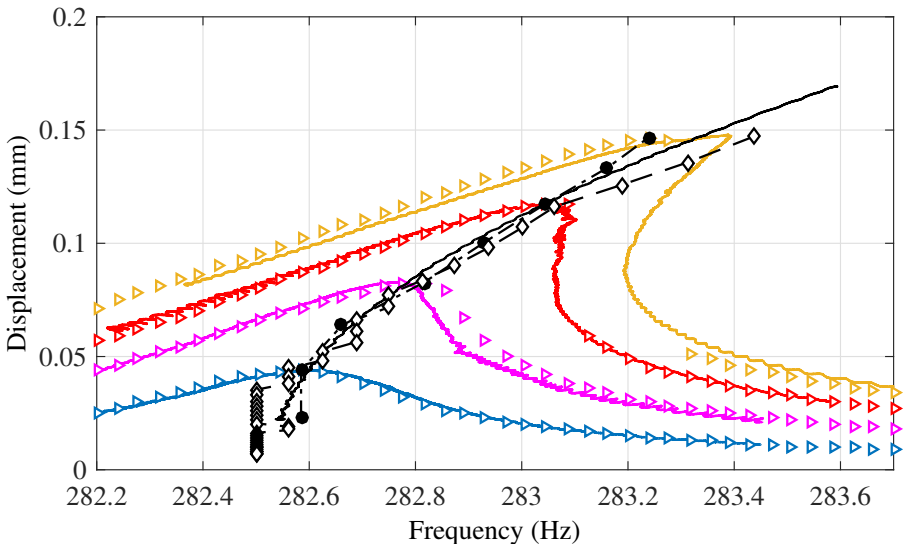

Figure 11 – Mode (0,1) of the gong: backbone curves obtained using PLL (solid black), using NLRD (black lozenge), using SST (filled black circles), forced frequency responses measured with PLL (colored line) under currents 0.1 (blue), 0.2 (purple), 0.3 (red) and 0.4 A (yellow). and forced frequency responses measured with SST(colored triangle) under currents 0.1 (blue), 0.2 (purple), 0.3 (red) and 0.4 A (yellow).

Fig. 12 shows that mode (1,1) has a also a hardening behaviour. Again, the frequency responses for different amplitudes are displayed and a larger multivalued region appears for the forcing amplitudes tested in this case. The nonlinear identification for mode (1,1) yields the parameters indicated in Tab. 2. Comparing modes (0,1) and (1,1), it appears that the measurements on mode (0,1) were trickier : it is probably due to higher amplitudes, the appearance of solid body motion, and lower modal damping. The measurements made on mode (1,1) are much cleaner.

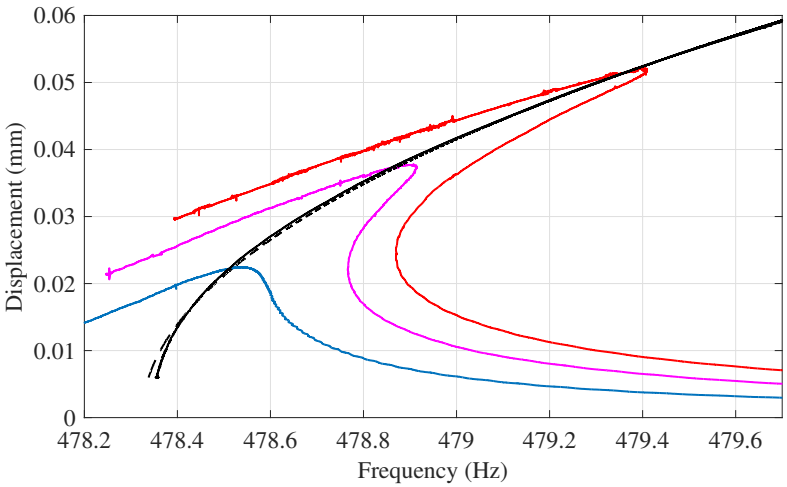

Figure 12 – Mode (1,1) of the gong: backbone curve (solid black), fitted parabola (dashed black) and forced frequency responses under current 0.185 (blue), 0.324 (purple) and 0.464 A (red) in the coil, using PLL.

	Mode (0,1)			Mode (1,1)
Method	PLL	NLRD	SST	PLL
f_0 (Hz)	282.53	282.49	282.55	478.32
$\hat{\Gamma}_0$ ($m^{-2}.s^{-2}$)	1.11×10^{12}	1.31×10^{12}	9.97×10^{11}	1.97×10^{13}

Table 2 – Experimentally identified nonlinear coefficients for mode (0,1) and (1.1) of the chinese gong.

4.4 Piezoelectric unimorph beams

Unimorph beams are often used in the context of energy harvesting [66] : in this domain, nonlinearities are interesting because of the incurvation of the frequency response with the amplitude, allowing to harvest vibration energy on wider frequency range [67]. There is thus a need for the identification of nonlinear parameters, especially for building a reasonable reduced-order model of the harvesting system. Moreover, in the case of piezoelectric devices, the modal electro-mechanical coupling coefficient k_i of the i-th. mode is an indicator of the performance and is linked to the natural frequencies ω_i^{OC} and ω_i^{SC} with the piezoelectric ceramic in open and short-circuit, respectively [68]:

$$k_i = \frac{(\omega_i^{\mathrm{OC}})^2 - (\omega_i^{\mathrm{SC}})^2}{(\omega_i^{\mathrm{SC}})^2}. \tag{46}$$

In the case of nonlinear unimorph beam, the frequencies depend on the excitation amplitude.

The unimorph studied here is constituted by a steel beam of dimensions 120 × 20 × 0.75 mm on which is glued a PZT ceramic PIC155 with dimension 20 × 60 × 0.5 mm. The placement and dimensions of the PZT ceramic are optimised for the first mode of the cantilever, according to [68]. The frequency responses for this unimorph beam in open and short-circuit around the first resonance are obtained for several vibration amplitudes using the PLL, set with an integral gain of 25 and a proportional gain of 1. They are plotted on Fig. 13. The tracked backbone curves for the two configurations are also plotted. For a given configuration (open or short-circuit), the estimated backbone curve is very accurate and seems to match the amplitude resonance, which is understandable since the damping is reasonably low. It is clear that the nonlinearity for the first mode is softening and the backbone curve is straight. The first mode of a base-excited cantilever beam is usually known to be hardening [69] but the softening behaviour may come from several phenomena: internal residual stress [70] due to the beam manufacturing process, or the coupling with the PZT ceramic are known to produce a softening behaviour [17]. Other possible reasons for this particular softening behavior are the quality of the clamping condition, which may generate dry friction, or the nonlinear nature of the shaker, interacting with the excited structure. Further study is needed to fully understand the nonlinear dynamic of this piezoelectric beam alone. Nonlinear piezoelectric cantilever beams are well studied in the literature [71, 72] and the key point may be in the modelisation of the piezoelectric ceramic nonlinearity: for instance, [72] enhances that straight backbones are observed for bimorph cantilever with soft piezoelectrics such as the PIC155 used here. Since the backbone curves are almost straight lines, one cannot identify a nonlinear cubic coefficient based on the model proposed in Sec. 2

No stabilized unstable region is observed, due to the quality factor and the small vibration amplitudes involved. High amplitudes were not tested; they were indeed more likely to damage the glueing of the PZT ceramic or the ceramic itself. The resonance shift between the two configurations is noticeable and quasi-constant when amplitude increases. From Eq. (46), it is found that k_1=19% for the first mode of the unimorph beam under study, which demonstrates the quality of the coupling between beam and ceramic and makes the structure attractive for energy harvesting.

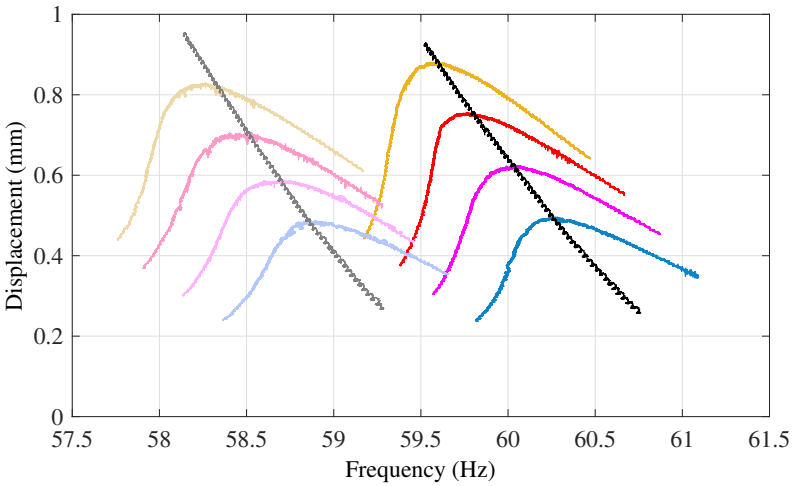

Figure 13 – Forced frequency responses using PLL for mode 1 of the piezoelectric unimorph beam in open (bright tone) and short-(light tone) circuit for base accelerations 0.90 (blue), 1.20 (purple), 1.50 (red), 1.80 (yellow) m.s^{-2}, and corresponding backbone curves for open (black) and short- (gray) circuit.

5 Conclusions

This paper is dedicated to the identification of nonlinear modes using the phase resonance method and a phase-locked-loop. A framework has been proposed to identify a single nonlinear mode based on displacement measurements at moderate amplitudes. An isolated nonlinear mode is characterized by two nonlinear cubic coefficients, whose effects are impossible to distinguish at first order. Hence, it was proposed to characterized a nonlinear mode with a linear eigenfrequency and a single nonlinear coefficient. These two parameters are identified by fitting a parabola on the measured backbone curve of the mode.

The strategy retained to measure the backbone curve is the phase resonance technique. It is done practically using a Phase-Locked-Loop. The PLL can also be used to measure nonlinear forced responses around resonance by maintaining the amplitude constant and varying the phase. The stability of the controlled nonlinear oscillator is demonstrated for any value of the phase lag, thus avoiding the jump phenomenon appearing in the classical stepped sine sweep method. Stability is dependent on the characteristics of the nonlinear oscillator, the gain and the speed of the feedback loop. The use of the PLL and more generally the phase resonance technique in case of internal resonances should be studied further. The evaluation of the stability of the measured backbone could also be studied.

The proposed method is applied in this paper to identify two nonlinear hardening modes of a circular plate, two nonlinear hardening modes of a chinese gong and the first flexural softening mode of a unimorph piezoelectric beam. Backbone curves and frequency responses are measured in each case. The unstable region of the frequency response is also measured. Except in the case of the piezoelectric beam, fitting a parabola on the backbone curves allowed a reliable estimation of the two parameters characterizing the nonlinear modes. In the case of the circular plate, the nonlinear coefficients are successfully compared with the theoretical coefficients. The piezoelectric beam displays an unexpected nonlinear behaviour, which does not allow to identify a nonlinear coefficient. This should be investigated in a further study.

In addition, two other measurement methods are used in order to identify the nonlinear modes and assess the validity of the phase resonance testing : a stepped sine sweep measurement and the nonlinear resonant decay method. The three methods yields identical results but in this study, the phase resonance method using PLL seems to give the cleanest result, since it is done in forced regime, and does not rely on an instantaneous frequency detection algorithm nor the measurement of a high number of forced frequency responses.

References

[1] R. J. Allemang, D. L. Brown, Experimental modal analysis, in: A. G. Piersol, T. L. Paez (Eds.), Shock and vibration handbook, McGraw-Hill, 2009.

[2] J.-P. Noël, G. Kerschen, Nonlinear system identification in structural dynamics: 10 more years of progress, Mechanical Systems and Signal Processing 83 (2016) 2–35.

[3] G. Kerschen, K. Worden, A. F. Vakakis, J.-C. Golinval, Past, present and future of nonlinear system identification in structural dynamics, Mechanical Systems and Signal Processing 20 (3) (2006) 505–592.

[4] K. Worden, G. R. Tomlinson, Nonlinearity in structural synamics. Detection, identification and modelling, IOP Publishing Ltd., 2001.

[5] A. H. Nayfeh, D. T. Mook, Nonlinear oscillations, John Wiley & sons, inc., New-York, 1979.

[6] A. Lazarus, O. Thomas, J. F. Deü, Finite element reduced order models for nonlinear vibrations of piezoelectric layered beams with applications to NEMS, Finite Elements in Analysis and Design 49 (1) (2012) 35–51.

[7] O. Thomas, B. Legrand, C. Fuinel, Optimization of length and thickness of smart transduction layers on beam structures for control and m/nems applications, in: Proceedings of SMASIS 2015 (ASME 2015 Conference on Smart Materials Adaptive Structures and Intelligent Systems), Colorado Springs, USA, 2015, p. paper 8857.

[8] M. K. Samal, P. Seshu, S. Parashar, U. Von Wagner, P. Hagedorn, B. K. Dutta, H. S. Kushwaha, A finite element model for nonlinear behaviour of piezoceramics under weak electric fields, Finite Elements in Analysis and Design 41 (15) (2005) 1464–1480.

[9] L. Jezequel, C. Lamarque, Analysis of non-linear dynamical systems by the normal form theory, Journal of Sound and Vibration 149 (3) (1991) 429–459.

[10] C. Touzé, O. Thomas, a. Chaigne, Hardening/softening behaviour in non-linear oscillations of structural systems using non-linear normal modes, Journal of Sound and Vibration 273 (1-2) (2004) 77–101.

[11] C. Touzé, O. Thomas, Non-linear behaviour of free-edge shallow spherical shells: Effect of the geometry, International Journal of Non-Linear Mechanics 41 (5) (2006) 678–692.

[12] M. Amabili, Nonlinear Vibrations and Stability of Shells and Plates, Cambridge University Press, 2008.

[13] O. Thomas, C. Touzé, A. Chaigne, Non-linear vibrations of free-edge thin spherical shells: modal interaction rules and 1:1:2 internal resonance, International Journal of Solids and Structures 42 (11-12) (2005) 3339–3373.

[14] C. Touzé, C. Camier, G. Favraud, O. Thomas, Effect of imperfections and damping on the type of nonlinearity of circular plates and shallow spherical shells, Mathematical Problems in Engineering 2008 (2008) ID 678307.

[15] O. Thomas, F. Mathieu, W. Mansfield, C. Huang, S. Trolier-Mckinstry, L. Nicu, Efficient parametric amplification in micro-resonators with integrated piezoelectric actuation and sensing capabilities, Applied Physics Letters 102 (16) (2013) 163504.

[16] N. Kacem, J. Arcamone, F. Perez-Murano, S. Hentz, Dynamic range enhancement of nonlinear nanomechanical resonant cantilevers for highly sensitive nems gas/mass sensor applications, Journal of Micromechanics and Microengineering 20 (4) (2010) 045023.

[17] M. K. Samal, P. Seshu, S. Parashar, U. von Wagner, P. Hagedorn, B. K. Dutta, S. Kushwaha, A finite element model for nonlinear behaviour of piezoceramics under weak electric fields, Finite Elements in Analysis and Design.

[18] S. Mojrzisch, J. Twiefel, Phase-controlled frequency response measurement of a piezoelectric ring at high vibration amplitude, Archive of Applied Mechanics 86 (10) (2015) 1763–1769.

[19] S. Peter, R. I. Leine, Excitation power quantities in phase resonance testing of nonlinear systems with phase-locked-loop excitation, Mechanical Systems and Signal Processing 96 (2017) 139–158.

[20] O. Thomas, C. Touzé, A. Chaigne, Asymmetric non-linear forced vibrations of free-edge circular plates. Part II: Experiments, Journal of Sound and Vibration 265 (5) (2003) 1075–1101.

[21] M. P. Mignolet, A. Przekop, S. A. Rizzi, S. M. Spottswood, A review of indirect/non-intrusive reduced order modeling of nonlinear geometric structures, Journal of Sound and Vibration 332 (2013) 2437–2460.

[22] A. Sénéchal, Réduction de vibrations de structure complexe par shunts piézoélectriques : application aux turbomachines, Ph.D. thesis, Conservatoire National des Arts et Métiers, Paris (2011).

[23] C. Touzé, M. Vidrascu, D. Chapelle, Direct finite element computation of non-linear modal coupling coefficients for reduced-order shell models, Computational Mechanics 54 (2) (2014) 567–580.

[24] M. Géradin, D. Rixen, Mechanical Vibrations: Theory and Applications to Structural Dynamics, 3rd Edition, J. Wiley & Sons, 2015.

[25] A. A. Muravyov, S. A. Rizzi, Determination of nonlinear stiffness with application to random vibration of geometrically nonlinear structures, Computers and Structures 81 (15) (2003) 1513–1523.

[26] O. Thomas, S. Bilbao, Geometrically nonlinear flexural vibrations of plates: In-plane boundary conditions and some symmetry properties, Journal of Sound and Vibration 315 (3) (2008) 569–590.

[27] C. Camier, C. Touzé, O. Thomas, Non-linear vibrations of imperfect free-edge circular plates and shells, European Journal of Mechanics A/Solids 28 (3) (2009) 500–515.

[28] C. Touzé, M. Amabili, Nonlinear normal modes for damped geometrically nonlinear systems: Application to reduced-order modelling of harmonically forced structures, Journal of Sound and Vibration 298 (4-5) (2006) 958–981.

[29] G. Kerschen, M. Peeters, J. C. Golinval, A. F. Vakakis, Nonlinear normal modes, Part I: A useful framework for the structural dynamicist, Mechanical Systems and Signal Processing 23 (1) (2009) 170–194.

[30] C. Touzé, O. Thomas, A. Huberdeau, Asymptotic non-linear normal modes for large-amplitude vibrations of continuous structures, Computers and Structures 82 (31-32) (2004) 2671–2682.

[31] C. Touzé, M. Amabili, O. Thomas, Reduced-order models for large-amplitude vibrations of shells including in-plane inertia, Computer Methods in Applied Mechanics and Engineering 197 (21-24) (2008) 2030–2045.

[32] S. W. Shaw, C. Pierre, Nonlinear normal modes and invariant manifolds, Journal of Sound and Vibration 150 (1) (1991) 170–173.

[33] S. W. Shaw, C. Pierre, Normal Modes of Vibration for Non-Linear Continuous Systems, Journal of Sound and Vibration 169 (3) (1994) 319–347.

[34] R. M. Rosenberg, On non-linear vibrations of systems with many degrees of freedom, Advances in Applied Mechanics 9 (1966) 155–242.

[35] A. M. Lyapunov, Problème général de la stabilité du mouvement, Annales de la faculté des sciences de Toulouse, 2^{e} série 9 (1907) 203–474, http://www.numdam.org/item?id=AFST_1907_2_9__203_0.

[36] A. F. Kelley, Analytic two-dimensional subcenter manifolds for systems with an integral, Pacific Journal of Mathematics 29 (2) (1969) 335–350.

[37] G. Haller, S. Ponsioen, Nonlinear normal modes and spectral submanifolds: existence, uniqueness and use in model reduction, Nonlinear Dynamics 86 (3) (2016) 1493–1534.

[38] O. Thomas, C. Touzé, E. Luminais, Modèles réduits de structures minces en vibrations non-linéaires, in: Colloque national en calcul de structure, Giens, 2005, pp. 1–6.

[39] M. Monteil, O. Thomas, C. Touzé, Identification of mode couplings in nonlinear vibrations of the steelpan, Applied Acoustics 89 (2015) 1–15.

[40] R. Arquier, B. Cochelin, S. Karkar, A. Lazarus, O. Thomas, C. Vergez, MANLAB 2.0, an interactive continuation software (2010).
URL `http://manlab.lma.cnrs-mrs.fr`

[41] J. R. Wright, J. E. Cooper, M. J. Desforges, Normal-mode force appropriation - theory and application, Mechanical Syatems and Signal Processing 13 (2) (1999) 217–240.

[42] M. Peeters, G. Kerschen, J. C. Golinval, Dynamic testing of nonlinear vibrating structures using nonlinear normal modes, Journal of Sound and Vibration 330 (3) (2011) 486–509.

[43] S. Baguet, B. Cochelin, Determination of branches of limit points by an asymptotic numerical method, in: European Congress on Computational Methods in Applied Sciences and Engineering, ECCOMAS 2000, no. September, 2000, pp. 11–14.

[44] A. Renault, O. Thomas, H. Mahé, Y. Lefebvre, Hardening / softening behaviour of antiresonance for nonlinear torsional vibration absorbers, in: Proc. of the 24th. International Congress on Theoretical and Applied Mechanics, Montreal, Canada, 2016.

[45] O. Thomas, C. Touzé, A. Chaigne, Non-linear behaviour of gongs through the dynamics of simple rods systems, in: Proceedings of ISMA, Perugia, Italy, 2001.

[46] M. Peeters, G. Kerschen, J. C. Golinval, Modal testing of nonlinear vibrating structures based on nonlinear normal modes: Experimental demonstration, Mechanical Systems and Signal Processing 25 (4) (2011) 1227–1247.

[47] J. M. Londoño, S. A. Neild, J. E. Cooper, Identification of backbone curves of nonlinear systems from resonance decay responses, Journal of Sound and Vibration 348 (2015) 224–238.

[48] D. A. Ehrhardt, M. S. Allen, Measurement of nonlinear normal modes using multi-harmonic stepped force appropriation and free decay, Mechanical Systems and Signal Processing 76-77 (2016) 612–633.

[49] S. Peter, R. Riethmüller, R. I. Leine, Tracking of backbone curves of nonlinear systems using phase-locked-loops, in: Conference Proceedings of the Society for Experimental Mechanics Series, Vol. 1, 2016, pp. 107–120.

[50] I. J. Sokolov, V. I. Babitsky, Phase control of self-sustained vibration, Journal of Sound and Vibration 248 (4) (2001) 725–744.

[51] S. Mojrzisch, J. Wallaschek, J. Bremer, An Experimental Method for the Phase Controlled Frequency Response Measurement of Nonlinear Vibration Systems, Pamm 12 (1) (2012) 253–254.

[52] J. Sieber, B. Krauskopf, Control based bifurcation analysis for experiments, Nonlinear Dynamics 51 (3) (2008) 365–377.

[53] E. Bureau, F. Schilder, M. Elmegård, I. F. Santos, J. J. Thomsen, J. Starke, Experimental bifurcation analysis of an impact oscillator-Determining stability, Journal of Sound and Vibration 333 (21) (2014) 5464–5474.

[54] L. Renson, A. Gonzalez-Buelga, D. A. W. Barton, S. A. Neild, Robust identification of backbone curves using control-based continuation, Journal of Sound and Vibration 367 (2016) 145–158.

[55] D. A. W. Barton, Control-based continuation: Bifurcation and stability analysis for physical experiments, Mechanical Systems and Signal Processing 84 (2017) 54–64.

[56] O. Thomas, C. Touzé, É Luminais, Non-linear vibrations of free-edge thin spherical shells: Experiments on a 1:1:2 internal resonance, Nonlinear Dynamics 49 (1-2) (2007) 259–284.

[57] J. Twiefel, M. Klubal, C. Paiz, S. Mojrzisch, H. Krüger, Digital signal processing for an adaptive phase-locked loop controller, Proceedings of SPIE 6926 (2008) 69260A.

[58] Zurich Intruments, Principles of lock-in detection and the state of the art (Nov. 2016).
URL `https://www.zhinst.com/applications/principles-of-lock-in-detection`

[59] M. Fan, M. Clark, Z. C. Feng, Implementation and stability study of phase-locked-loop nonlinear dynamic measurement systems, Communications in Nonlinear Science and Numerical Simulation 12 (7) (2007) 1302–1315.

[60] J. A. Sanders, F. Verhulst, J. Murdock, Averaging Methods in Nonlinear Dynamical Systems, Second Edition, springer Edition, 2007.

[61] C. Touzé, O. Thomas, A. Chaigne, Asymmetric non-linear forced vibrations of free-edge circular plates. Part I: Theory, Journal of Sound and Vibration 258 (4) (2002) 649–676.

[62] P. S. Varoto, L. P. R. de Oliveira, On the force drop off phenomenon in shaker testing in experimental modal analysis, Shock and Vibration 9 (2002) 165–175.

[63] A. I. Manevitch, L. I. Manevitch, Free oscillations in conservative and dissipative symmetric cubic two-degree-of-freedom systems with closed natural frequencies, Meccanica 38 (2003) 335–338.

[64] N. H. Fletcher, Nonlinear frequency shifts in quasispherical-cap shells: Pitch glide in Chinese gongs, Journal of the Acoustical Society of America 78 (6) (1985) 2069–2073.

[65] T. D. Rossing, N. H. Fletcher, Nonlinear vibrations in plates and gong, The Journal of the Acoustical Society of America 73 (January) (1983) 345–351.

[66] S. R. Anton, H. A. Sodano, A review of power harvesting using piezoelectric materials, Smart Materials and Structures 16 (3) (2007) R1–R21.

[67] M. F. Daqaq, R. Masana, A. Erturk, D. Dane Quinn, On the Role of Nonlinearities in Vibratory Energy Harvesting: A Critical Review and Discussion, Applied Mechanics Reviews 66 (4) (2014) 040801.

[68] J. Ducarne, O. Thomas, J. F. Deü, Placement and dimension optimization of shunted piezoelectric patches for vibration reduction, Journal of Sound and Vibration 331 (14) (2012) 3286–3303.

[69] P. F. Pai, A. H. Nayfeh, Non-linear non-planar oscillations of a cantilever beam under lateral base excitations, International Journal of Non-Linear Mechanics 25 (5) (1990) 455–474.

[70] L. G. Villanueva, R. B. Karabalin, M. H. Matheny, D. Chi, J. E. Sader, M. L. Roukes, Nonlinearity in nanomechanical cantilevers, Physical Review B - Condensed Matter and Materials Physics 87 (2013) 024304.

[71] S. N. Mahmoodi, M. F. Daqaq, N. Jalili, On the nonlinear-flexural response of piezoelectrically driven microcantilever sensors, Sensors and Actuators, A: Physical 153 (2) (2009) 171–179.

[72] S. Leadenham, A. Erturk, Unified nonlinear electroelastic dynamics of a bimorph piezoelectric cantilever for energy harvesting, sensing, and actuation, Nonlinear Dynamics 79 (2015) 1727–1743.

Appendix A Dimensionless coefficients for the circular plate

A clever way to compute the nonlinear coefficients of the NNMs of a given circular plate is to formulate the plate's equations of motion in terms of dimensionless variable, so that the computation is done for a generic circular plate. Here, following Ref. [61], we use the dimensionless variables:

$$\bar{u} = \frac{R}{h^2}u, \tag{47}$$

and

$$\bar{t} = \frac{\sqrt{D/\rho h}}{R^2}t, \tag{48}$$

where R is the radius of the plate, h its the thickness, E is the Young's modulus, ρ is the mass density and ν is the Poisson ratio of the plate's material, and $D = Eh^3/12(1-\nu^2)$, in order to rewrite Eq. (15) in the following form:

$$\ddot{\bar{u}} + \bar{\omega}^2\dot{\bar{u}} + \varepsilon\bar{\Gamma}\bar{u}^3 = 0, \tag{49}$$

with

$$\varepsilon = 12(1-\nu^2)h^2/R^2. \tag{50}$$

It is then possible to identify the dimensionless frequency $\bar{\omega}$:

$$\bar{\omega} = R^2\sqrt{\frac{\rho h}{D}}\omega_0, \tag{51}$$

and dimensionless nonlinear cubic coefficient $\bar{\Gamma}$:

$$\bar{\Gamma} = \frac{\rho R^4}{E}\Gamma_0. \tag{52}$$

In the case of the circular plate studied in Sec. 4, the following values are used for the parameters : E=85$\times$ 10^9 Pa, ρ=7974 kg.m^{-3}, ν=0.38, h=1.6 mm and R=110 mm.